RESEARCH ARTICLE | DECEMBER 12 2014

Efficient field-theoretic simulation of polymer solutions

Michael C. Villet; Glenn H. Fredrickson

J. Chem. Phys. 141, 224115 (2014)
https://doi.org/10.1063/1.4902886
CHORUS

Efficient field-theoretic simulation of polymer solutions

Michael C. Villet[1] and Glenn H. Fredrickson[1,2,3,a)]
[1]*Department of Chemical Engineering, University of California, Santa Barbara, California 93106, USA*
[2]*Department of Materials, University of California, Santa Barbara, California 93106, USA*
[3]*Materials Research Laboratory, University of California, Santa Barbara, California 93106, USA*

(Received 12 October 2014; accepted 17 November 2014; published online 12 December 2014)

We present several developments that facilitate the efficient field-theoretic simulation of polymers by complex Langevin sampling. A regularization scheme using finite Gaussian excluded volume interactions is used to derive a polymer solution model that appears free of ultraviolet divergences and hence is well-suited for lattice-discretized field theoretic simulation. We show that such models can exhibit *ultraviolet sensitivity*, a numerical pathology that dramatically increases sampling error in the continuum lattice limit, and further show that this pathology can be eliminated by appropriate model reformulation by variable transformation. We present an exponential time differencing algorithm for integrating complex Langevin equations for field theoretic simulation, and show that the algorithm exhibits excellent accuracy and stability properties for our regularized polymer model. These developments collectively enable substantially more efficient field-theoretic simulation of polymers, and illustrate the importance of simultaneously addressing analytical and numerical pathologies when implementing such computations. © *2014 AIP Publishing LLC*. [http://dx.doi.org/10.1063/1.4902886]

I. INTRODUCTION

Since its introduction by Edwards in the 1960s,[1] field-theoretic polymer modeling has proven to be a powerful tool for both the analytic and numerical study of equilibrium polymer physics. In particular, numerical implementation of self-consistent field theory (SCFT) has enabled enormous progress in the understanding of self-assembly of block copolymers.[2–4] However, the mean-field approximation intrinsic to SCFT calculations breaks down when strong fluctuations are present, such as in polymer solutions, polyelectrolytes, and polymer melts near critical points. Field-theoretic simulation using complex Langevin (CL) sampling[5,6] offers a scalable and highly general computational methodology for studying such systems, as was first demonstrated by Ganesan and Fredrickson;[7] this method has subsequently been used to study confined polymer solutions,[8,9] polyelectrolyte complexation,[10–12] and the order-disorder transition in diblock copolymer melts.[7,13]

Despite the potential of the field-theoretic simulation approach, several numerical and theoretical barriers have slowed the widespread use of this method. Initial studies were hindered by a need for small timesteps to stably and accurately integrate the Langevin equations of the CL method. Lennon *et al.*[14] showed that semi-implicit algorithms offer dramatically improved stability, and found that predictor-corrector schemes can be used to improve accuracy. However, accuracy and stability constraints still may limit useful timesteps to well below the correlation time of the system; improved algorithms thus offer the potential for faster equilibration and sampling, and hence lower-cost simulations.

More troubling for the field-theoretic simulation methodology are the presence of *ultraviolet divergences* in polymer field theories. These are theoretical pathologies in which the functional integrals in field-theoretic polymer partition functions are divergent; the "ultraviolet" moniker, which originates from quantum field theory, indicates that insufficiently damped high-frequency modes of the integrand are responsible for the divergence. In field-theoretic simulation, these pathologies manifest as an extreme sensitivity to the choice of lattice discretization, with properties such as the free energy and chemical potential diverging as simulation lattices are refined towards the continuum limit.[9] Relative free energy calculations are still possible with careful use of reference states,[13] but this linkage to the details of the computational lattice complicates the interpretation of simulation results and poses serious theoretical barriers to the use of advanced numerical techniques such as variable cell shapes, multigrid methods, and systematic coarse-graining.

In this paper, we present several developments that facilitate the efficient and easily interpretable field-theoretic simulation of polymer solutions. We detail a Gaussian regularization framework that analytically controls ultraviolet divergences, allowing field-theoretic simulations to access a well-behaved continuum limit. A related numerical pathology that interferes with the measurement of the osmotic pressure, which we term ultraviolet sensitivity, is further discussed and addressed. Finally, we describe an exponential differencing algorithm for integrating complex Langevin equations that offers excellent stability and accuracy properties compared to existing methods. These methodologies are introduced in the context of the Edwards model of homopolymer in implicit solvent, but are directly applicable to broader classes of multicomponent, heterogeneous, and charged polymer systems, both in solution and melt conditions. Taken together, these developments represent a substantial improvement on current "best practice" for the field-theoretic simulation of polymers, and we hope they will facilitate the broader adoption of

a)Electronic mail: ghf@mrl.ucsb.edu

complex Langevin simulations for the study of fluctuating polymer systems.

II. ULTRAVIOLET DIVERGENCE MANAGEMENT

In this section, we present a framework for conducting field-theoretic simulations free of pathological behavior in the continuum limit. We first present a regularized polymer solution model that can be used to conduct ultraviolet divergence-free field theoretic simulations. We then describe a pathology that we call *ultraviolet sensitivity* in which numerical calculations that approach the continuum limit incur additional sampling error, and show how this pathology can be eliminated via appropriate rescaling of the field variables. Simulation results illustrating the techniques described in this section are provided in Sec. IV, following the discussion of complex Langevin field-theoretic simulation methods in Sec. III.

A. The Gaussian-regularized Edwards model

Perhaps the most minimal polymer field theory is the venerable Edwards model for homopolymer chains in good solvent.[15] Despite its simplicity, the mathematical features of this model are archetypical of more complicated field theories, and so it serves as a useful platform for methods development and evaluation. As noticed by Edwards, this field theory has an ultraviolet divergence originating from infinite monomeric self-interaction energies. We here present a regularized form of the Edwards model with finite self-interactions, but which includes the divergent Edwards model as a limiting case.

The Edwards model field theory can be derived from a particle-based description of homopolymer in implicit solvent. We consider a polymer solution in the canonical ensemble, with n identical polymer chains in a volume V at temperature T. Each polymer chain j is described by a space curve $\mathbf{r}_j(s)$, $s \in [0, N]$, where s is a contour variable indexing positions of a continuous string of monomers; we denote the set of these space curves $\{\mathbf{r}_j(s)\}$ by $\mathbf{r}^{nN}$. The canonical partition function of this polymer system is a Boltzmann-weighted integral over all $\mathbf{r}^{nN}$:

$$Z_C(n, V, T) = \frac{1}{n!\left(\lambda_T^3\right)^{nN}} \prod_{j=1}^{n} \int D\mathbf{r}_j \, e^{-\beta U_0[\mathbf{r}^{nN}] - \beta \bar{U}[\mathbf{r}^{nN}]}, \tag{1}$$

where $\beta = 1/k_B T$, λ_T is the de Broglie wavelength, $U_0[\mathbf{r}^{nN}]$ is an energy functional for short-range intramolecular energetics, and $\bar{U}[\mathbf{r}^{nN}]$ is an energy functional for long-range and intermolecular non-bonded energetics. The functional integrals $\int D\mathbf{r}_j$ denote path integration over all possible space curves for a given polymer j.

Intramolecular bond energies are described with the continuous Gaussian chain model, i.e., the harmonic stretching potential $U_0[\mathbf{r}^{nN}] = \frac{3k_B T}{2b^2} \sum_{j=1}^{n} \int_0^N ds \left|\frac{d\mathbf{r}_j(s)}{ds}\right|^2$, where b is a bond length scale.

The non-bonded potentials (of mean force) are assumed to be pairwise amongst monomers:

$$\bar{U}[\mathbf{r}^{nN}] = \frac{1}{2} \sum_{j=1}^{n} \sum_{k=1}^{n} \int_0^N ds \int_0^N ds' \, \bar{u}(\mathbf{r}_j(s) - \mathbf{r}_k(s')), \tag{2}$$

where for $j = k$ the integrals exclude the self-interaction contributions $s = s'$. Such interactions contain important physical content for some systems, such as solvated electrolytes in a spatially varying dielectric field,[16] but for a translationally invariant system the self-interactions can be factored out of the configuration integrals, acting as a reference shift to the free energy. Nevertheless, divergent self-interactions ultimately introduce ultraviolet divergences into the subsequently derived field theory, as we will see shortly.

The standard Edwards model uses a Dirac delta function for pairwise interactions, $\bar{u}(\mathbf{r} - \mathbf{r}') = u_0 \, \delta(\mathbf{r} - \mathbf{r}')$, with u_0 an interaction strength parameter. This purely repulsive potential is a simple model for solvent-mediated excluded volume interaction; in conjunction with the continuous Gaussian chain backbone, the model is able to capture many universal features of polymer solutions.[15] Moreover, the corresponding partition function is readily convertible to a statistical field theory by means of a formally exact mathematical procedure, the Hubbard-Stratonovich transform.

To apply this transform, the interaction potential $\bar{U}[\mathbf{r}^{nN}]$ is expressed as a quadratic integral by introducing the monomer position density $\hat{\rho}(\mathbf{r}) \equiv \sum_{j=1}^{n} \int_0^N ds \, \delta(\mathbf{r} - \mathbf{r}_j(s))$:

$$\bar{U}[\mathbf{r}^{nN}] = \frac{1}{2} \int d\mathbf{r} \int d\mathbf{r}' \, \hat{\rho}(\mathbf{r}) \bar{u}(\mathbf{r} - \mathbf{r}') \hat{\rho}(\mathbf{r}') - \frac{1}{2} nN \, \bar{u}(\mathbf{0}). \tag{3}$$

The quadratic integral includes self-interactions; to maintain consistency with (2), we must subtract the self-interaction energy $nN\bar{u}(\mathbf{0})/2$, which for the Edwards model is infinite in magnitude. The inclusion of an infinite self-interaction in the quadratic integral is the source of ultraviolet divergence in the ensuing field theory. To control this divergence, we regularize the theory by replacing the Dirac delta with a Gaussian interaction potential that is finite on contact; the Edwards model is readily recoverable as a limit of this Gaussian potential.

Rather than directly using a Gaussian form for $\bar{u}(\mathbf{r} - \mathbf{r}')$, we use a mathematically equivalent regularization introduced by Wang to study electrolyte solutions.[16] In Wang's scheme, point charges are replaced by Gaussian charge distributions of unit integral, thus regularizing electrostatic self-interaction energies. For our uncharged model, each monomer is treated not as a point mass but as the center of a Gaussian density distribution; this distributed mass then interacts by a delta function potential.

Mathematically, we define a monomeric mass distribution function with unit volume integral, $\Gamma(\mathbf{r}) = \frac{\exp(-|\mathbf{r}|^2/2a^2)}{(2\pi)^{3/2} a^3}$, where a is a monomeric length scale. The mass density $\check{\rho}(\mathbf{r})$ is then given by the convolution of this distribution function with the monomer position density, $\check{\rho}(\mathbf{r}) = \Gamma * \hat{\rho}(\mathbf{r}) \equiv \int d\mathbf{r}' \, \Gamma(\mathbf{r} - \mathbf{r}') \, \hat{\rho}(\mathbf{r}')$.

The mass density replaces the monomer position density in the total interaction potential (3):

$$\bar{U}[\mathbf{r}^{nN}] = \frac{1}{2}\int d\mathbf{r}\int d\mathbf{r}'\,\check{\rho}(\mathbf{r})\bar{u}(\mathbf{r}-\mathbf{r}')\check{\rho}(\mathbf{r}') - \frac{1}{2}nN\,\bar{u}_S[\Gamma], \tag{4}$$

where $\bar{u}_S[\Gamma]$ is the monomeric self-energy, $\bar{u}_S[\Gamma] = \int d\mathbf{r}\int d\mathbf{r}'\,\Gamma(\mathbf{r})\,\bar{u}(\mathbf{r}-\mathbf{r}')\,\Gamma(\mathbf{r}') = \frac{u_0}{8\pi^{3/2}a^3}$. The limit $a \to 0$ recovers the Edwards model; $\bar{u}_S[\Gamma]$ is divergent in this limit.

This interaction potential is equivalent to an effective soft repulsive interaction between point monomers located at $\mathbf{r}_0$ and $\mathbf{r}_0'$ of $\bar{u}_{\text{eff}}(\mathbf{r}_0-\mathbf{r}_0') = \int d\mathbf{r}\int d\mathbf{r}'\,\Gamma(\mathbf{r}-\mathbf{r}_0)\,\bar{u}(\mathbf{r}-\mathbf{r}')\,\Gamma(\mathbf{r}'-\mathbf{r}_0') = \bar{u}_S[\Gamma]\,e^{-\frac{|\mathbf{r}_0-\mathbf{r}_0'|^2}{4a^2}}$, and thus the distributed-density regularization is entirely equivalent to using a Gaussian pairwise interaction directly; the corresponding field theories are related to each other by a variable transformation. However, we consider the distributed-density regularization framework to be preferable for two reasons. First, the field theory that emerges naturally from the distributed-density regularization offers superior numerical performance for reasons we discuss briefly in Sec. II E. Second, as shown by Wang's work,[16,17] the distributed-monomer formalism offers a physically motivated regularization scheme for field theories of electrostatic species, and is thus natural to use when extending the model considered here to treat polyelectrolyte solutions.[12]

We now proceed with the Hubbard-Stratonovich transform, which uses a Gaussian functional integral identity to rewrite the exponentiated interaction energy:

$$e^{-\frac{\beta}{2}\int d\mathbf{r}\,d\mathbf{r}'\,\check{\rho}(\mathbf{r})\bar{u}(\mathbf{r}-\mathbf{r}')\check{\rho}(\mathbf{r}')} = \frac{\int D\omega\, e^{-\frac{1}{2\beta}\int d\mathbf{r}\,d\mathbf{r}'\,\omega(\mathbf{r})\bar{u}^{-1}(\mathbf{r}-\mathbf{r}')\omega(\mathbf{r}')-i\int d\mathbf{r}\,\omega(\mathbf{r})\check{\rho}(\mathbf{r})}}{\int D\omega\, e^{-\frac{1}{2\beta}\int d\mathbf{r}\,d\mathbf{r}'\,\omega(\mathbf{r})\bar{u}^{-1}(\mathbf{r}-\mathbf{r}')\omega(\mathbf{r}')}} \tag{5}$$

where $\bar{u}^{-1}(\mathbf{r})$ is the functional inverse of $\bar{u}(\mathbf{r})$, defined by $\int d\mathbf{r}'\,\bar{u}(\mathbf{r}-\mathbf{r}')\,\bar{u}^{-1}(\mathbf{r}'-\mathbf{r}'') = \delta(\mathbf{r}-\mathbf{r}'')$; this inverse must exist and be positive definite for this identity to hold. For our interaction potential, these conditions are satisfied, with $\bar{u}^{-1}(\mathbf{r}) = u_0^{-1}\delta(\mathbf{r})$.

We employ this identity to rewrite the partition function (1):

$$\begin{aligned} Z_C(n,V,T) &= \frac{1}{n!\left(\lambda_T^3\right)^{nN}}\prod_{j=1}^{n}\int D\mathbf{r}_j\, e^{-\beta U_0[\mathbf{r}^{nN}]}e^{-\frac{\beta}{2}\int d\mathbf{r}\,d\mathbf{r}'\,\check{\rho}(\mathbf{r})\bar{u}(\mathbf{r}-\mathbf{r}')\check{\rho}(\mathbf{r}')}e^{\beta nN\bar{u}_S[\Gamma]/2} \\ &= \frac{e^{\beta nN\bar{u}_S[\Gamma]/2}}{n!\left(\lambda_T^3\right)^{nN}}\prod_{j=1}^{n}\int D\mathbf{r}_j\, e^{-\beta U_0[\mathbf{r}^{nN}]}\frac{\int D\omega\, e^{-\frac{1}{2\beta}\int d\mathbf{r}\,d\mathbf{r}'\,\omega(\mathbf{r})\bar{u}^{-1}(\mathbf{r}-\mathbf{r}')\omega(\mathbf{r}')-i\int d\mathbf{r}\,\omega(\mathbf{r})\check{\rho}(\mathbf{r})}}{\int D\omega\, e^{-\frac{1}{2\beta}\int d\mathbf{r}\,d\mathbf{r}'\,\omega(\mathbf{r})\bar{u}^{-1}(\mathbf{r}-\mathbf{r}')\omega(\mathbf{r}')}} \\ &= \frac{e^{\beta nN\bar{u}_S[\Gamma]/2}}{n!\left(\lambda_T^3\right)^{nN}}\frac{\int D\omega\, e^{-\frac{1}{2\beta u_0}\int d\mathbf{r}\,\omega(\mathbf{r})^2}\prod_{j=1}^{n}\int D\mathbf{r}_j\, e^{-\beta U_0[\mathbf{r}^{nN}]-i\int d\mathbf{r}\,\Gamma*\omega(\mathbf{r})\hat{\rho}(\mathbf{r})}}{\int D\omega\, e^{-\frac{1}{2\beta u_0}\int d\mathbf{r}\,\omega(\mathbf{r})^2}}, \end{aligned} \tag{6}$$

where we have used the fact that $\Gamma(\mathbf{r})$ is a function only of $|\mathbf{r}|$ to rewrite $\int d\mathbf{r}\,\omega(\mathbf{r})\check{\rho}(\mathbf{r}) = \int d\mathbf{r}\,\Gamma * \omega(\mathbf{r})\,\hat{\rho}(\mathbf{r})$.

We now simplify further by factoring the intramolecular energies of independent chains:

$$\begin{aligned} &\prod_{j=1}^{n}\int D\mathbf{r}_j\, e^{-\beta U_0[\mathbf{r}^{nN}]}e^{-i\int d\mathbf{r}\,\Gamma*\omega(\mathbf{r})\hat{\rho}(\mathbf{r})} \\ &= \prod_{j=1}^{n}\int D\mathbf{r}_j\, e^{-\frac{3}{2b^2}\int_0^N ds\left|\frac{d\mathbf{r}_j(s)}{ds}\right|^2-i\int d\mathbf{r}\,\Gamma*\omega(\mathbf{r})\int_0^N ds\,\delta(\mathbf{r}-\mathbf{r}_j(s))} \\ &= \left(\int D\mathbf{r}\, e^{-\frac{3}{2b^2}\int_0^N ds\left|\frac{d\mathbf{r}(s)}{ds}\right|^2-i\int_0^N ds\,\Gamma*\omega(\mathbf{r}(s))}\right)^n \\ &\equiv \left(Z_0\,Q[i\Gamma*\omega]\right)^n. \end{aligned} \tag{7}$$

Above, we have defined Z_0 to be the partition function of a single ideal continuous Gaussian chain in the absence of any potential, and the functional $Q[\Omega]$ to be the normalized partition function of a single continuous Gaussian chain in an applied chemical potential field $\Omega(\mathbf{r})$:

$$Z_0 = \int D\mathbf{r}\,\exp\left(-\frac{3}{2b^2}\int_0^N ds\left|\frac{d\mathbf{r}(s)}{ds}\right|^2\right), \tag{8}$$

$$Q[\Omega] = Z_0^{-1}\int D\mathbf{r}\,\exp\left(-\frac{3}{2b^2}\int_0^N ds\left|\frac{d\mathbf{r}(s)}{ds}\right|^2 - \int_0^N ds\,\Omega(\mathbf{r}(s))\right). \tag{9}$$

The auxiliary field $\omega(\mathbf{r})$ introduced by the Hubbard-Stratonovich transformation is purely real; therefore, $Q[i\Gamma*\omega(\mathbf{r})]$ has a purely imaginary argument, and the Hubbard-Stratonovich transform naturally introduces a complex integrand into the partition function.

With single-chain partition functions thus defined, we can compactly express the transformed partition function of the Edwards model:

$$Z_C(n,V,T) = \frac{{Z_0}^n}{n!\left(\lambda_T^3\right)^{nN}}e^{\beta nN\bar{u}_S[\Gamma]/2} \times \frac{\int D\omega\, e^{-\frac{1}{2\beta u_0}\int d\mathbf{r}\,\omega(\mathbf{r})^2+n\ln Q[i\Gamma*\omega]}}{\int D\omega\, e^{-\frac{1}{2\beta u_0}\int d\mathbf{r}\,\omega(\mathbf{r})^2}}. \tag{10}$$

We simplify further by introducing the rescaled variables $\mathbf{x} = \mathbf{r}/R_g$, $\sigma = s/N$, $w = N\omega$, $\alpha = a/R_g$, $\tilde{V} = V/R_g^3$, and $B = \frac{\beta u_0 N^2}{R_g^3}$ where $R_g = (Nb^2/6)^{1/2}$ is the ideal-chain radius of

gyration. Use of these variables suppresses dependencies on N and b, with B serving as a control parameter for the strength of excluded volume interactions:

$$Z_C(n,V,T) = \frac{{Z_0}^n}{n!\left(\lambda_T^3\right)^{nN}} e^{\beta n N \bar{u}_S[\Gamma]/2} \times \frac{\int Dw\, e^{-\frac{1}{2B}\int d\mathbf{x}\, w(\mathbf{x})^2 + n\ln Q[i\Gamma * w]}}{\int Dw\, e^{-\frac{1}{2B}\int d\mathbf{x}\, w(\mathbf{x})^2}}, \quad (11)$$

$$Q[W] = \frac{\int D\mathbf{x}\, \exp\left(-\frac{1}{4}\int_0^1 d\sigma \left|\frac{d\mathbf{x}(\sigma)}{d\sigma}\right|^2 - \int_0^1 d\sigma\, W(\mathbf{x}(\sigma))\right)}{\int D\mathbf{x}\, \exp\left(-\frac{1}{4}\int_0^1 d\sigma \left|\frac{d\mathbf{x}(\sigma)}{d\sigma}\right|^2\right)}. \quad (12)$$

For convenient reference, we now divide the partition function into constituent components:

$$Z_C(n,V,T) \equiv Z_{\text{ig}}(n,V,T)\, Z_S(n,T)\, \frac{\mathcal{Z}(n,\tilde{V},B)}{\mathcal{Z}_0(\tilde{V},B)}, \quad (13)$$

$$\begin{aligned} Z_{\text{ig}}(n,V,T) &= {Z_0}^n/n!(\lambda_T^3)^{nN}, \\ Z_S(n,T) &= e^{\beta n N \bar{u}_S[\Gamma]/2}, \\ \mathcal{Z}(n,\tilde{V},B) &= \int Dw\, \exp(-H[w]), \\ \mathcal{Z}_0(\tilde{V},B) &= \int Dw\, e^{-\frac{1}{2B}\int d\mathbf{x}\, w(\mathbf{x})^2}, \end{aligned} \quad (14)$$

where $H[w]$, referred to as the effective Hamiltonian, is

$$H[w] = \frac{1}{2B}\int d\mathbf{x}\, w(\mathbf{x})^2 - n\ln Q[i\Gamma * w]. \quad (15)$$

Each of these contributing terms is handled separately in computation. $Z_{\text{ig}}(n,V,T)$ is the partition function of an ideal gas of ideal, non-interacting continuous Gaussian chains. The logarithm of this partition function is divergent, due to the vanishing of the functional integral over chain space curves in Z_0 for the continuous Gaussian chain.[3] This ultraviolet divergence in the chain contour variable is inherent to the continuous Gaussian chain model; a fully convergent field theory can be derived using a bead-spring chain model instead. However, well-defined physical predictions can be obtained by calculating excess properties, which quantify deviations from the ideal-gas reference state described by Z_{ig}.

These deviations from ideality, originating from excluded-volume interactions, are described by the remaining contributions to Z_C. Of greatest importance is the field-theoretic partition function $\mathcal{Z}(n,\tilde{V},T)$, a highly nontrivial functional integral that is the central object of interest in polymer field theory. $\mathcal{Z}$ is formally divergent unless divided by $\mathcal{Z}_0$, a Gaussian functional integral that acts as a normalization factor.

The final contribution to the partition function, Z_S, contains only self-interaction effects. However, as our original particle-based formulation of $Z_C(n,V,T)$ specifically excluded self-interactions, Z_S is in reality a correction to the presence of artificially introduced self-interactions in $\mathcal{Z}/\mathcal{Z}_0$, carried forward from the rewriting of the interaction potential as a quadratic integral in (4). Given that $Z_C(n,V,T)$ is finite even in the limit of a delta function interaction, the divergence of Z_S as $\alpha = a/R_g \to 0$ necessitates that $\mathcal{Z}/\mathcal{Z}_0$ will diverge as well; this is the origin of the ultraviolet divergences in the field theory.

Having obtained a field-theoretic partition function, we use thermodynamic relations to calculate excess properties. The Helmholtz free energy is

$$\begin{aligned} A(n,V,T) &= -k_BT\, \log Z_C(n,V,T) \\ &= -k_BT\, \log Z_{\text{ig}} - k_BT\, \log\left(Z_S\, \frac{\mathcal{Z}}{\mathcal{Z}_0}\right) \\ &\equiv A_{\text{ig}}(n,V,T) + A_{\text{ex}}(n,V,T). \end{aligned} \quad (16)$$

Thermodynamic properties computed from derivatives of this free energy are readily divisible into ideal and excess contributions. Two important such properties in the canonical ensemble are the excess chemical potential $\mu_{\text{ex}}(n,V,T)$ and excess osmotic pressure $\Pi_{\text{ex}}(n,V,T)$.

The excess chemical potential is given by

$$\begin{aligned} \beta\mu_{\text{ex}}(n,V,T) &= \frac{\partial}{\partial n}\beta A_{\text{ex}}(n,V,T) \\ &= \frac{\int Dw\, e^{-H[w]}\log Q[i\Gamma * w]}{\int Dw\, e^{-H[w]}} - \frac{\beta N \bar{u}_S[\Gamma]}{2} \\ &\equiv \langle \log Q[i\Gamma * w]\rangle - \frac{\beta N \bar{u}_S[\Gamma]}{2}, \end{aligned} \quad (17)$$

where $\langle\,\rangle$ interprets the functional integral ratio in (17) as an ensemble average over field configurations $w(\mathbf{x})$ with "probability" weights provided by $H[w]$. Because $H[w]$ is complex-valued, this is not a true probability distribution, in which each field configuration would have a strictly real probability; however, it has a mathematical form otherwise identical to that of a traditional statistical field theory.

We see from Eq. (17) that $\tilde{\mu}[w] \equiv \log Q[i\Gamma * w]$ serves as a field-theoretic *operator* for the excess chemical potential: an ensemble average over field configurations provides the chemical potential of the original particle-based theory. A similar field-theoretic operator can be derived for the excess osmotic pressure by executing a volume derivative:

$$\begin{aligned} \beta R_g^3\, \Pi_{\text{ex}}(n,V,T) &= -\frac{\partial}{\partial\tilde{V}}\beta A_{\text{ex}}(n,V,T) \\ &= \left\langle \frac{\partial H[w]}{\partial\tilde{V}}\right\rangle + \frac{\partial}{\partial\tilde{V}}\log\mathcal{Z}_0(\tilde{V},B) \\ &= \frac{1}{2B\tilde{V}}\left\langle \int d\mathbf{x}\, w(\mathbf{x})^2\right\rangle \\ &\quad - n\left\langle \frac{\frac{\partial Q[i\Gamma * w]}{\partial\tilde{V}}}{Q[i\Gamma * w]}\right\rangle + \frac{\partial\log\mathcal{Z}_0}{\partial\tilde{V}}, \end{aligned} \quad (18)$$

$$\frac{\partial Q[i\Gamma * w]}{\partial\tilde{V}} = -\frac{1}{V}\int d\mathbf{x}\left(\frac{2}{3}\Phi_\nabla(\mathbf{x};[i\Gamma * w]) + (i\Gamma_2 * w(\mathbf{x}))\Phi(\mathbf{x};[i\Gamma * w])\right), \quad (19)$$

where Eq. (19) and the functions $\Phi(\mathbf{x};[W])$, $\Phi_\nabla(\mathbf{x};[W])$, and $\Gamma_2(\mathbf{x})$ are derived in Appendix B. Unlike the excess chemical potential, the normalization integral $\mathcal{Z}_0(\tilde{V}, B)$ contributes to the excess osmotic pressure; this has important consequences that will be discussed in Sec. II D.

With a field-theoretic form for the Gaussian-regularized Edwards model (henceforth abbreviated as the GREM) in hand, we will now study directly how the divergences that have been alluded to in this section manifest in analytic and numerical computations.

B. Ultraviolet divergences in the Edwards model

In Sec. II A, we saw that the excess free energy, and hence all excess thermodynamic properties, can be calculated for the Gaussian-regularized Edwards model from the field theoretic partition function $\mathcal{Z}(n, \tilde{V}, B)$, the normalization integral $\mathcal{Z}_0(\tilde{V}, B)$, and the self-energy correction $Z_S(n, B)$. We have already obtained an analytic form for Z_S, which diverges exponentially as $\alpha \to 0$. The functional integral in $\mathcal{Z}$ cannot be evaluated analytically without approximation, but the normalization integral $\mathcal{Z}_0$ is Gaussian and so can be calculated analytically.

Executing the functional integrals $\int Dw$ requires a function space for $w(\mathbf{x})$; recalling that functional integrals were introduced into the partition function via the identity (5), we are at liberty to choose a function space consistent with that identity. We choose the space of square-integrable functions with periodic boundary conditions in a cubic box of R_g-scaled side length $\tilde{L} = \tilde{V}^{-\frac{1}{3}}$, for which we can employ the standard periodic Fourier basis:

$$\begin{aligned} w(\mathbf{x}) &= \frac{1}{\tilde{V}} \sum_{\mathbf{k}} \hat{w}_{\mathbf{k}}\, e^{i\mathbf{k}\cdot\mathbf{x}}, \\ \hat{w}_{\mathbf{k}} &= \int d\mathbf{x}\, w(\mathbf{x}) e^{-i\mathbf{k}\cdot\mathbf{x}} \end{aligned} \tag{20}$$

with $\hat{w}_{\mathbf{k}}$ the Fourier coefficients and $\mathbf{k}$ the reciprocal lattice vectors $\mathbf{k} = \frac{2\pi}{\tilde{L}}(j_1\hat{\mathbf{x}} + j_2\hat{\mathbf{y}} + j_3\hat{\mathbf{z}})$ where $j_i = 0, \pm1, \pm2, \cdots, \pm\infty$ for $i = 1, 2, 3$. As $w(\mathbf{x})$ is real-valued, the (complex-valued) Fourier modes are not independent from their complex conjugates, with $\hat{w}^*_{\mathbf{k}} = \hat{w}_{-\mathbf{k}}$.

We now define the functional integral as the integral over all values of all independent Fourier coefficients

$$\int Dw = \int_{-\infty}^{\infty} \frac{d\hat{w}_{\mathbf{0}}}{\sqrt{2}} \prod_{\mathbf{k}\in\mathcal{K}} \int_{-\infty}^{\infty} d\hat{w}^R_{\mathbf{k}} \int_{-\infty}^{\infty} d\hat{w}^I_{\mathbf{k}}, \tag{21}$$

where the set $\mathcal{K}$ is a half-space of $\mathbf{k}$ modes that excludes $\mathbf{k} = 0$, and we have introduced a normalization factor of $\sqrt{2}$ for future notational convenience.

With this definition, we can integrate a generic Gaussian functional integral of the form:

$$\begin{aligned} \mathcal{G} &\equiv \int Dw\, \exp\left[-\frac{1}{2V}\sum_{\mathbf{k}} \gamma_k\, \hat{w}_{\mathbf{k}}\, \hat{w}_{-\mathbf{k}}\right] \\ &= \int Dw\, \exp\left[-\frac{\gamma_0}{2V}\hat{w}^2_{\mathbf{0}} - \frac{1}{V}\sum_{\mathbf{k}\in\mathcal{K}} \gamma_k\left(\left(\hat{w}^R_{\mathbf{k}}\right)^2 + \left(\hat{w}^I_{\mathbf{k}}\right)^2\right)\right] \\ &= \int_{-\infty}^{\infty} \frac{d\hat{w}_{\mathbf{0}}}{\sqrt{2}}\, e^{-\frac{1}{2V}\gamma_0\hat{w}^2_{\mathbf{0}}} \prod_{\mathbf{k}\in\mathcal{K}} \int_{-\infty}^{\infty} d\hat{w}^R_{\mathbf{k}}\, e^{-\frac{1}{V}\gamma_k\left(\hat{w}^R_{\mathbf{k}}\right)^2} \\ &\quad \times \int_{-\infty}^{\infty} d\hat{w}^I_{\mathbf{k}}\, e^{-\frac{1}{V}\gamma_k\left(\hat{w}^I_{\mathbf{k}}\right)^2} \\ &= \sqrt{\frac{\pi V}{\gamma_0}} \prod_{\mathbf{k}\in\mathcal{K}} \sqrt{\frac{\pi V}{\gamma_k}} \sqrt{\frac{\pi V}{\gamma_k}} \\ &= \prod_{\mathbf{k}} \sqrt{\frac{\pi V}{\gamma_k}}, \end{aligned} \tag{22}$$

where γ_k is assumed to be a real-valued function of the wavevector magnitude $k = |\mathbf{k}|$. In carrying out this calculation, the necessary summation of duplicate modes within the half space $\mathcal{K}$ introduces a factor of 2 that is not always accounted for in prior literature.[3,18]

We can use this result to analytically integrate $\mathcal{Z}_0(\tilde{V}, B)$:

$$\begin{aligned} \mathcal{Z}_0(\tilde{V}, B) &= \int Dw\, e^{-\frac{1}{2B}\int d\mathbf{x}\, w(\mathbf{x})^2} \\ &= \int Dw\, e^{-\frac{1}{2B\tilde{V}}\sum_{\mathbf{k}} \hat{w}_{\mathbf{k}}\hat{w}_{-\mathbf{k}}} \\ &= \prod_{\mathbf{k}} \sqrt{\pi\tilde{V}B}, \end{aligned} \tag{23}$$

which is evidently divergent in the continuum limit, where there are an infinite number of $\mathbf{k}$ modes.

Although $\mathcal{Z}$ cannot be integrated exactly, it can be studied by asymptotic analysis about saddle points of the integrand, where

$$\frac{\delta H[w]}{\delta w(\mathbf{x})} = \frac{w(\mathbf{x})}{B} - n\frac{\delta \ln Q[i\Gamma * w]}{\delta w(\mathbf{x})} = 0. \tag{24}$$

This integrand has a homogeneous saddle point at $w(\mathbf{x}) = -iBn/\tilde{V} \equiv -iBC$, where we have defined the overall chain density $C = n/\tilde{V}$. Using a weak inhomogeneity expansion detailed in Appendix A, asymptotic expansion of $H[w]$ in powers of w about this saddle point yields

$$\begin{aligned} H[w] \sim{}& \frac{BC^2\tilde{V}}{2} + \frac{1}{2B\tilde{V}}\sum_{\mathbf{k}} \hat{w}_{\mathbf{k}}\hat{w}_{-\mathbf{k}} \\ &+ \frac{C}{2\tilde{V}}\sum_{\mathbf{k}\neq 0} \hat{g}_D(k^2)\hat{\Gamma}(k)^2 \hat{w}_{\mathbf{k}}\hat{w}_{-\mathbf{k}} \end{aligned} \tag{25}$$

to quadratic order, where $\hat{g}_D(x)$ is the Fourier-transformed Debye function $\hat{g}_D(x) = \frac{2}{x^2}(e^{-x} - 1 + x)$.

Referring to the Gaussian integration formula (22), we obtain

$$\mathcal{Z} \sim \sqrt{\pi\tilde{V}B} \prod_{\mathbf{k}\neq 0} \sqrt{\frac{\pi\tilde{V}}{B^{-1} + C\,\hat{g}_D(k^2)e^{-\alpha^2k^2}}}, \tag{26}$$

$$\frac{\mathcal{Z}}{\mathcal{Z}_0} \sim \prod_{\mathbf{k}\neq 0} \left(1 + BC\,\hat{g}_D(k^2)e^{-\alpha^2k^2}\right)^{-\frac{1}{2}}, \tag{27}$$

where we have made use of the fact that $\hat{\Gamma}(k) = e^{-\alpha^2k^2/2}$.

This asymptotic approximation to the field-theoretic partition function, a so-called *one-loop* result in the perturbation

framework of quantum field theory, can now be used to calculate the excess free energy:

$$\beta A_{\rm ex} \sim -\frac{\beta n N \bar{u}_S[\Gamma]}{2} + \frac{BC^2\tilde{V}}{2} + \frac{1}{2}\sum_{\mathbf{k}\neq 0} \log\left[1 + BC\,\hat{g}_D(k^2)e^{-\alpha^2 k^2}\right] \quad (28)$$

$$\approx -\frac{\beta n N \bar{u}_S[\Gamma]}{2} + \frac{BC^2\tilde{V}}{2} + \frac{1}{2}\frac{\tilde{V}}{(2\pi)^3}\int d\mathbf{k}\, \log\left[1 + BC\,\hat{g}_D(k^2)e^{-\alpha^2 k^2}\right] \quad (29)$$

$$\approx -\frac{\beta n N \bar{u}_S[\Gamma]}{2} + \frac{BC^2\tilde{V}}{2} + \frac{\tilde{V}}{4\pi^2}\int_0^{\Lambda} dk\, k^2 \log\left[1 + BC\,\hat{g}_D(k^2)e^{-\alpha^2 k^2}\right], \quad (30)$$

where we have assumed a large-volume limit to approximate the sum over $\mathbf{k}$ by an integral in (29), and in (30) have artificially introduced a high-frequency cutoff Λ.

For large k, the integrand in (30) decays as $\sim e^{-\alpha^2 k^2}$, which for $\alpha > 0$ is sufficiently quickly for the integral to converge even as $\Lambda \to \infty$, and at the one-loop level the field theory is finite. However, for $\alpha = 0$, the integrand no longer decays rapidly enough at large k and the integral diverges for $\Lambda \to \infty$; no well-defined continuum free energy exists! This pathology is called an "ultraviolet" divergence because its origin is the insufficiently rapid decay of high-frequency contributions to the free energy. Either a finite-width Gaussian potential of $\alpha > 0$ or a finite high-wavevector cutoff Λ serves to regularize these short-range interactions; however, the $\alpha > 0$ regularization has a clear physical interpretation in the original polymer solution model. In contrast, the physical ramifications of introducing an ad-hoc Λ cutoff to the field theory are far less clear.

The one-loop free energy can be differentiated to obtain one-loop approximations for the chemical potential and osmotic pressure:

$$\beta\mu_{\rm ex} \sim -\frac{\beta N \bar{u}_S[\Gamma]}{2} + BC + \frac{1}{2\tilde{V}}\sum_{\mathbf{k}\neq 0}\frac{B\hat{g}_D(k^2)e^{-\alpha^2 k^2}}{1 + BC\,\hat{g}_D(k^2)e^{-\alpha^2 k^2}}, \quad (31)$$

$$\beta R_g^3\,\Pi_{\rm ex} \sim \frac{BC^2}{2} - \frac{1}{2\tilde{V}}\sum_{\mathbf{k}\neq 0}\left(\log\left[1 + BC\,\hat{g}_D(k^2)e^{-\alpha^2 k^2}\right] - \frac{BC\,\hat{g}_D(k^2)e^{-\alpha^2 k^2}}{1 + BC\,\hat{g}_D(k^2)e^{-\alpha^2 k^2}}\right). \quad (32)$$

The summand in the one-loop chemical potential (31) scales as $\sim k^{-2}e^{-\alpha^2 k^2}$ for large k, which is convergent for $\alpha > 0$ but not for $\alpha = 0$, and so the chemical potential is also ultraviolet divergent. However, the summand in the one-loop osmotic pressure (32) scales as $\sim k^{-4}e^{-2\alpha^2 k^2}$ for large k, which is ultraviolet convergent even for $\alpha = 0$.

This convergent osmotic pressure illustrates that field theories can offer useful physical insight even if they are ultraviolet divergent. Furthermore, one-loop free energy and chemical potential *differences* between states of identical B but differing n or C are ultraviolet convergent, and so reference states can be employed to obtain finite values of these properties. In addition to reference state subtraction, more sophisticated renormalization approaches are also available for analytically managing ultraviolet divergences in polymer field theories, in which ultraviolet divergent contributions are identified and incorporated into renormalized model parameters.[19–21]

It is essential for the utility of polymer field theory that ultraviolet divergences are controllable in this manner. The divergences originate from short-range interactions, which the coarse-grained pair potentials employed in polymer field theory are not intended to treat accurately. If properties sensitive to the fine-grained details of intermolecular interactions are to be investigated, then a more realistic molecular model must be used. Fortunately, many universal polymer properties are independent of such molecular detail.

It is also important to note that the one-loop approximation is just the leading term in a systematic loop expansion in the parameter $(B/C)^{1/2}$ (small in the concentrated regime of $C \gg B$); it is possible for additional divergences to exist in higher-order terms, or indeed for divergent individual terms to sum to a convergent full field theory. In field-theoretic simulations, all orders of the field theory are sampled, but the discretization of the field theory onto a simulation lattice automatically introduces a high-wavevector cutoff regularization; we now explore the consequences of ultraviolet divergences for numerical analysis in detail.

C. Ultraviolet divergences in computational field theory

We have already seen that analytic evaluation of $\mathcal{Z}(n, \tilde{V}, B)$ cannot be carried out exactly, even for this simple physical system. Numerical techniques offer a valuable alternative, but require discretization of the continuous field $w(\mathbf{x})$ onto a finite-dimensional vector space suitable for computational use.

For our periodic system, we impose a uniform cubic lattice of points $\mathbf{r}$ with associated field values $w_{\mathbf{r}}$, each of which can take values $-\infty < w_{\mathbf{r}} < \infty$, with M_L lattice points per side and $M = M_L^3$ total points. This real-space basis has the discrete Fourier transform

$$w_{\mathbf{x}} = \frac{1}{\tilde{V}}\sum_{\mathbf{k}} \hat{w}_{\mathbf{k}}\, e^{i\mathbf{k}\cdot\mathbf{x}}, \quad \hat{w}_{\mathbf{k}} = \Delta\tilde{V}\sum_{\mathbf{x}} w_{\mathbf{x}}\, e^{-i\mathbf{k}\cdot\mathbf{x}}, \quad (33)$$

where $\Delta\tilde{V} = \tilde{V}/M$ is the volumetric lattice spacing, and the reciprocal space includes wavevectors $\mathbf{k} = \frac{2\pi}{\tilde{L}}(j_1\hat{\mathbf{x}} + j_2\hat{\mathbf{y}} + j_3\hat{\mathbf{z}})$ where $j_i = 0, \pm 1, \pm 2, \cdots, \pm\frac{M_L - 1}{2}$ for $i = 1, 2, 3$ and odd M_L (for even M_L, the j_i range from $-(\frac{M_L}{2} - 1)$ to $+\frac{M_L}{2}$). The real-space representation $w_{\mathbf{x}}$ and Fourier representation $\hat{w}_{\mathbf{k}}$ describe an identical vector space with M degrees of freedom. We will refer to the lattice spacing in each dimension as $\Delta x = L/M_L$.

The discretization of the function space results in a finite dimensional integral for the partition function, which through change of variables can be expressed either in either real or

Fourier representations:

$$\int Dw = (2\Delta\tilde{V})^{-\frac{M}{2}} \prod_{\mathbf{r}} \int_{-\infty}^{\infty} dw_{\mathbf{x}} = \int_{-\infty}^{\infty} \frac{d\hat{w}_{\mathbf{0}}}{\sqrt{2}} \prod_{\mathbf{k}\in\mathcal{K}} \int_{-\infty}^{\infty} d\hat{w}_{\mathbf{k}}^{R} \int_{-\infty}^{\infty} d\hat{w}_{\mathbf{k}}^{I}. \quad (34)$$

In this expression we have placed a Jacobian factor $(2\Delta\tilde{V})^{-\frac{M}{2}}$ in front of the real-space integral to maintain consistency with our continuum definition (21). The Gaussian integration formula (22) is directly applicable to the discrete case, albeit with the product over **k** now over the finite reciprocal lattice.

The introduction of this discrete vector space immediately regularizes our field theory; the limitation of the function space to a finite set of modes is a direct numerical analogue to the introduction of a high-frequency cutoff Λ in our analytic calculations. We note that even though only $\mathcal{Z}$ will be studied in a field-theoretic simulation, the integral $\mathcal{Z}_0$ must be discretized onto the same basis to obtain properly normalized results.

As for the continuum case, we can perform one-loop analysis on the discretized field theory: $A_{\rm ex}$, $\mu_{\rm ex}$ and $\Pi_{\rm ex}$ have the same form as the continuum results (28), (31) and (32), but with **k** summations over the finite lattice. As for our continuum Λ cutoff, the one-loop free energy and chemical potential are ultraviolet divergent in the continuum lattice limit for $\alpha = 0$ but convergent for $\alpha > 0$, while the osmotic pressure is convergent even for $\alpha = 0$.

In Figure 1, we plot lattice one-loop values of $\langle\tilde{\mu}\rangle = \mu_{\rm ex} + \beta N \bar{u}_s[\Gamma]/2$ and $\beta R_g^3 \Pi_{\rm ex}$ calculated by executing the sums (31) and (32) for $B = C = 1$, $L = 3.2\,R_g$ and varying α and Δx. We observe the expected divergence in the chemical potential for $\alpha = 0$; for finite α the divergence is truncated, with convergence reached for lattice resolutions Δx somewhat larger than the smearing radius α. For the osmotic pressure, the $\alpha = 0$ standard Edwards model converges quite slowly, with the summation over **k** modes still visibly converging on the continuum limit even for $\Delta x = 0.01$, a spatial resolution far smaller than is desirable to resolve for such a coarse-grained polymer model. As for the chemical potential, the one-loop osmotic pressure at finite α converges for Δx larger than α. We see that GREM displays smaller osmotic pressure for smaller α, corresponding to larger (attractive) corrections to the concentrated solution mean-field limit as the scale of excluded volume interaction is reduced.

The discrete field theory may also be investigated by field-theoretic simulation, which includes loop corrections of all orders. Alexander-Katz *et al.*[9] found that the chemical potential of the Edwards model ($\alpha = 0$ of the GREM) was fully regularized by subtraction of the discrete one-loop chemical potential. However, this subtractive approach is not readily generalizable. For inhomogeneous polymer systems, one-loop analysis may be difficult or impossible, and higher-order divergences may exist. Furthermore, reliance on lattice discretization for regularization couples the short-wavelength physics of the polymer model with the choice of computational lattice; this seriously complicates the use of numerical methods that adjust the lattice, such as variable cell shapes, multigrid methods, or systematic coarse-graining.

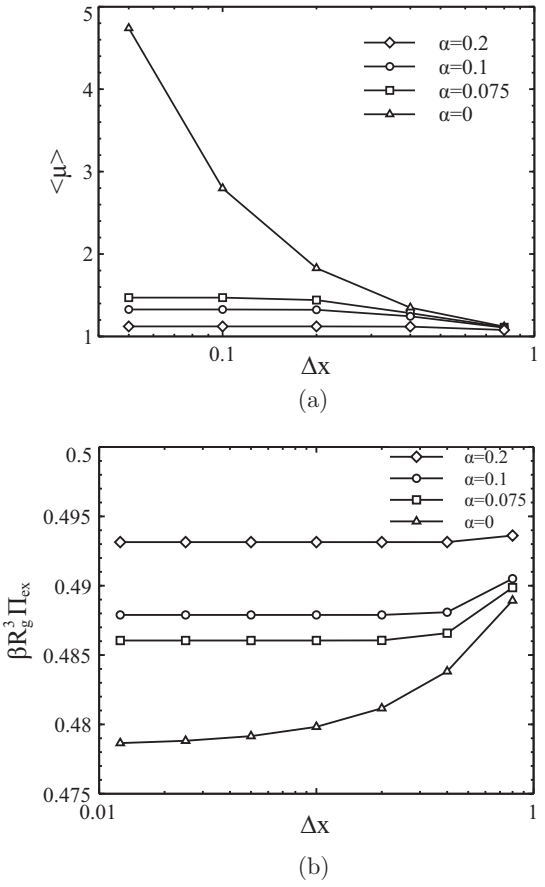

FIG. 1. Lattice discretization effects in lattice one-loop calculations of chemical potential and osmotic pressure of the GREM for $B = C = 1$ and $L = 3.2\,R_g$. (a) One-loop $\langle\tilde{\mu}\rangle = \mu_{\rm ex} + \beta N \bar{u}_s[\Gamma]/2$. (b) One-loop $\beta R_g^3 \Pi_{\rm ex}$.

In contrast, the finite Gaussian interaction potential used in the GREM guarantees a fully convergent field theory: the initial particle-based theory is fully finite (excepting the ultraviolet divergence in the chain contour, which affects only the ideal gas reference state), and as the Hubbard-Stratonovich transform is exact, the resulting field theory must be as well. For fixed α, the discretized GREM field theory will exhibit a well-defined continuum limit as the lattice is refined (as is confirmed in numerical tests in Sec. IV) and numerical methods operating within that continuum limit can vary their lattice spacing without affecting model physics. All sensitivity to short-range interactions is controlled analytically by the interaction range α, and the connection between the regularization scheme and the underlying particle-based model is fully transparent. Gaussian-regularized polymer models therefore offer a more physically transparent and numerically flexible platform for field theoretic simulation.

D. Ultraviolet sensitivity

We now discuss a numerical pathology associated with the continuum limit that affects calculation of the osmotic pressure. Returning to the osmotic pressure operator (18), we calculate the normalization contribution for our discrete

theory to be

$$\frac{\partial \log \mathcal{Z}_0}{\partial \tilde{V}} = \frac{\partial}{\partial \tilde{V}} \frac{M}{2} \log[\pi B \tilde{V}] = \frac{1}{2\Delta \tilde{V}}. \tag{35}$$

We can thus define the osmotic pressure operator

$$\tilde{\Pi} = \int d\mathbf{x} \left(\frac{w(\mathbf{x})^2}{2B} + \frac{n}{V} \frac{\frac{2}{3}\Phi_\nabla(\mathbf{x}; [i\Gamma * w]) + (i\Gamma_2 * w(\mathbf{x}))\Phi(\mathbf{x}; [i\Gamma * w])}{Q[i\Gamma * w]} \right) + \frac{1}{2\Delta \tilde{V}} \tag{36}$$

and calculate the excess osmotic pressure via the ensemble average $\beta R_g^3 \Pi_{ex} = \langle \tilde{\Pi} \rangle$.

With this operator, the osmotic pressure is calculated from the sum of an ensemble-averaged field correlation function of negative sign and an analytical positive signed term that diverges in the continuum limit of $\Delta \tilde{V} \to 0$. As Π_{ex} is expected to have a finite continuum limit, the averaged correlation function will necessarily grow larger and larger in magnitude as the lattice is refined, and must be measured to higher and higher decimal precision to obtain an equivalently accurate value for Π_{ex}. The need for higher precision necessitates longer simulation runs, and potentially smaller contour integration and simulation timesteps; compounded with the additional computational cost already required for use of a high-resolution simulation lattice, the cost of simulations can rapidly become prohibitive. We refer to this phenomenon, in which the approach to the continuum limit introduces increasing numerical pathology despite yielding a finite result, as *ultraviolet sensitivity*.

Fortunately, it is possible to eliminate the ultraviolet sensitivity of the osmotic pressure operator by a suitable change of variables. Returning to our original expression for the excess osmotic pressure in (18),

$$\begin{aligned} \beta R_g^3 \Pi_{\text{ex}} &= -\frac{\partial}{\partial \tilde{V}} \log \frac{\mathcal{Z}(n, \tilde{V}, B)}{\mathcal{Z}_0(\tilde{V}, B)} \\ &= -\frac{\partial}{\partial \tilde{V}} \log \frac{\int Dw\, e^{-H[w]}}{\int Dw\, e^{-\frac{1}{2B}\int d\mathbf{x}\, w(\mathbf{x})^2}}, \end{aligned} \tag{37}$$

we introduce the variable transformation $w(\mathbf{x}) = \tilde{V}^{-\frac{1}{2}} \phi(\mathbf{x})$:

$$\begin{aligned} \beta R_g^3 \Pi_{\text{ex}} &= -\frac{\partial}{\partial \tilde{V}} \log \frac{\int D\phi\, e^{-H[\tilde{V}^{-1/2}\phi]}}{\int D\phi\, e^{-\frac{1}{2B\tilde{V}}\int d\mathbf{x}\, \phi(\mathbf{x})^2}} \\ &= \frac{\int D\phi \frac{\partial H[\tilde{V}^{-1/2}\phi]}{\partial \tilde{V}} e^{-H[\tilde{V}^{-1/2}\phi]}}{\int D\phi\, e^{-H[\tilde{V}^{-1/2}\phi]}} \\ &\quad + \frac{\partial}{\partial \tilde{V}} \log \int D\phi\, e^{-\frac{1}{2B\tilde{V}}\int d\mathbf{x}\, \phi(\mathbf{x})^2}, \end{aligned} \tag{38}$$

where the boundary derivatives vanish due to periodicity. The second term in (38) is identically zero, as can be shown by applying the functional integration formula (22); the first term includes the derivative

$$\begin{aligned} &\frac{\partial H[\tilde{V}^{-1/2}\phi]}{\partial \tilde{V}} \\ &= \frac{\partial}{\partial \tilde{V}} \left(\frac{1}{2B\tilde{V}} \int d\mathbf{x}\, \phi(\mathbf{x})^2 - n \log Q\left[\frac{i\Gamma * \phi}{\tilde{V}^{1/2}}\right] \right) \\ &= n \frac{\int d\mathbf{x} \left(\frac{2}{3}\Phi_\nabla \left(\mathbf{x}; \left[\frac{i\Gamma * \phi}{\tilde{V}^{1/2}}\right] \right) + \frac{i\left(\Gamma_2 - \frac{1}{2}\Gamma\right) * \phi(\mathbf{x})}{\tilde{V}^{1/2}} \Phi\left(\mathbf{x}; \left[\frac{i\Gamma * \phi}{\tilde{V}^{1/2}}\right] \right) \right)}{\tilde{V}\, Q\left[\frac{i\Gamma * \phi}{\tilde{V}^{1/2}}\right]} \end{aligned} \tag{39}$$

with the details of the volume differentiation provided in Appendix B. We then transform back from $\phi(\mathbf{x})$ to $w(\mathbf{x})$ to obtain a new ensemble-average expression for the osmotic pressure:

$$\begin{aligned} \beta R_g^3 \Pi_{\text{ex}} &= \frac{\int Dw \frac{\partial H[\tilde{V}^{-1/2}\phi]}{\partial \tilde{V}} e^{-H[w]}}{\int Dw\, e^{-H[w]}} \\ &= \left\langle n \frac{\int d\mathbf{x} \left(\frac{2}{3}\Phi_\nabla(\mathbf{x}; [i\Gamma * w]) + \left(i\left(\Gamma_2 - \frac{1}{2}\Gamma\right) * w(\mathbf{x}) \right) \Phi(\mathbf{x}; [i\Gamma * w]) \right)}{\tilde{V}\, Q[i\Gamma * w]} \right\rangle \equiv \langle \tilde{\Pi}_{\text{UV}} \rangle. \end{aligned} \tag{40}$$

Comparing $\tilde{\Pi}_{\text{UV}}$ to $\tilde{\Pi}$, we see that the field squared integral and the ultraviolet-sensitive normalization integral have both been eliminated, replaced by an integrated product of the smeared field and the functional $\Phi(\mathbf{x}; [i\Gamma * w])/Q[i\Gamma * w]$ (which serves as a density operator, as discussed in Appendix A). We will demonstrate the superior numerical performance of this operator in Sec. IV.

E. Model choice and algorithm stability

In our derivation of the GREM in Sec. II A, we commented that use of the Gaussian mass distribution regularization yielded a field theory with improved numerical properties compared to one derived from an equivalent Gaussian pointwise pair potential. The field theory obtained from direct Hubbard-Stratonovich transformation of the latter formulation has the field-theoretic Hamiltonian

$$H[w] = \frac{1}{2B\tilde{V}} \sum_{\mathbf{k}} \hat{w}_{\mathbf{k}}\, \hat{w}_{-\mathbf{k}}\, e^{\alpha^2 k^2} - n \log Q[iw], \tag{41}$$

which is related to our previous Hamiltonian (15) by a variable transform convolving the field with the function $\Gamma(\mathbf{x})$.

The Fourier transform of the field-theoretic "force" $\frac{\delta H[w]}{\delta w(\mathbf{r})}$ for this model contains a term linear in the Fourier-transformed field that is multiplied by a factor of $e^{\alpha^2 k^2}$; this extreme amplification of high-frequency Fourier modes both dramatically destabilizes Langevin sampling algorithms, as will be discussed in Sec. III B, and can introduce numerical precision difficulties for high-resolution calculations. As was previously seen in the ultraviolet sensitivity of the osmotic pressure operator, mathematically equivalent field-theoretic formulations of the same underlying polymer model can have radically different numerical properties, and so care should be taken to choose a numerically favorable formulation.

III. EXPONENTIAL DIFFERENCING FOR COMPLEX LANGEVIN FIELD THEORETIC SIMULATION

In this section, we briefly review the complex Langevin method for field theoretic simulation. We then introduce an efficient exponential differencing algorithm with excellent stability and accuracy properties.

A. The complex Langevin method

In our derivation of the GREM, we have seen that thermodynamic properties can be related to ensemble-averaged field theoretic operators. For the discretized field theory, these ensembles averages are of the form

$$X = \langle \tilde{X}(\mathbf{w}) \rangle = \frac{\int d\mathbf{w}\, \tilde{X}(\mathbf{w})\, e^{-H(\mathbf{w})}}{\int d\mathbf{w}\, e^{-H(\mathbf{w})}}, \tag{42}$$

where X is a thermodynamic property of interest, $\tilde{X}(\mathbf{w})$ is the corresponding operator, $\mathbf{w}$ is the vector of discrete field values, and $H(\mathbf{w})$ is the discretized effective Hamiltonian.

Unfortunately, the complex-valued nature of $H(\mathbf{w})$ interferes with standard Monte Carlo sampling methods for statistical theories. To date, the CL method has proven most successful for directly calculating these integrals without further analytic approximation. This method, proposed originally by Parisi[5] and Klauder,[6] is discussed in detail by Fredrickson.[3]

In complex Langevin sampling, field configuration values $\mathbf{w}$ are evolved in a "time" coordinate according to a set of Langevin equations; the dynamical values $\mathbf{w}(t)$ and functions thereof are analytically extended to the complex plane. These CL equations take the form

$$\frac{\partial w_{\mathbf{r}}(t)}{\partial t} = -\frac{\lambda}{\Delta\tilde{V}} \frac{\partial H(\mathbf{w})}{\partial w_{\mathbf{r}}(t)} + \eta_{\mathbf{r}}(t), \tag{43}$$

where $\eta_{\mathbf{r}}(t)$ are purely real Gaussian random variables that are uncorrelated ("white noise") both temporally and spatially:

$$\begin{aligned} \langle \eta_{\mathbf{r}}(t) \rangle_{\eta} &= 0, \\ \langle \eta_{\mathbf{r}}(t) \eta_{\mathbf{r}'}(t') \rangle_{\eta} &= \frac{2\lambda}{\Delta\tilde{V}} \delta_{\mathbf{r},\mathbf{r}'}\, \delta(t - t'), \end{aligned} \tag{44}$$

where the averaging brackets $\langle\,\rangle_{\eta}$ now refer to expectation values averaged over possible manifestations of the noise $\eta_{\mathbf{r}}(t)$. We have introduced a factor of $\Delta\tilde{V}$ compared to Fredrickson's discrete CL definitions to maintain notational consistency with the continuous-space form of the complex Langevin equations in Fredrickson *et al.*;[22] $\frac{1}{\Delta V} \frac{\partial H(\mathbf{w})}{\partial w_{\mathbf{r}}}$ acts as a discrete approximation for the functional derivative $\frac{\delta H[w]}{\delta w(\mathbf{r})}$.

After the CL equations have reached a steady state, CL time averages become equal to the ensemble averages of interest in the infinite sampling time limit:

$$\lim_{T\to\infty} \frac{1}{T} \int_0^T dt\, \tilde{X}(\mathbf{w}(t)) = \langle \tilde{X}(\mathbf{w}) \rangle, \tag{45}$$

where $\tilde{X}(\mathbf{w})$ is a generic field-theoretic operator of interest. Unfortunately, for general $H(\mathbf{w})$ there is no theoretical guarantee that the CL equations will converge to a steady state. However, practical experience applying the CL method to polymer field theory has been that attaining convergence is primarily a *numerical* problem, where sufficiently stable numerics are always able to converge to steady-state solution. Moreover, the results of such converged simulations have been in good agreement with theory where reliable analytic results are available; indeed, CL simulations of a Gaussian-core simple fluid were found to be in direct agreement with calculations for the same model by particle-based Monte Carlo simulation.[23] Given these observations, and the flexibility accorded by the method, CL appears to be the most suitable and practical strategy for sampling complex-valued polymer field theories.

B. Numerical methods

The complex Langevin equations (43) have no analytic solution for nontrivial $H(\mathbf{w})$ and so must be integrated numerically. In general, this requires discretization of the time coordinate into timesteps Δt and an update algorithm to determine $\mathbf{w}^{t+\Delta t}$ from $\mathbf{w}^t$ (and $\mathbf{w}$ at earlier timesteps if a multistep method is used). Ensemble averaged properties are then estimated from a discretized version of the CL time average (45):

$$\langle \tilde{X}(\mathbf{w}) \rangle_{\substack{T \\ \Delta t}} = \frac{\Delta t}{T} \sum_{n=1}^{N_T} \tilde{X}(\mathbf{w}^{n\Delta t}), \tag{46}$$

where the total simulation time is $T = N_T \Delta t$. In using $\langle \tilde{X}(\mathbf{w}) \rangle_{\substack{T \\ \Delta t}}$ to estimate $\langle \tilde{X}(\mathbf{w}) \rangle$, the CL method introduces both sampling error and time discretization error.

Sampling error addresses the approach of $\langle \tilde{X}(\mathbf{w})\rangle_{\substack{T\\ \Delta t}}$ to the infinite-time limit $\langle \tilde{X}(\mathbf{w})\rangle_{\substack{\infty\\ \Delta t}}$. As is typical in stochastic simulations, the field configurations generated by the CL dynamical trajectory $\mathbf{w}(t)$ will be correlated beneath some correlation time τ. The mean square sampling error decreases with increasing simulation time according to $(\langle \tilde{X}(\mathbf{w})\rangle_{\substack{T\\ \Delta t}} - \langle \tilde{X}(\mathbf{w})\rangle_{\substack{\infty\\ \Delta t}})^2 \sim \frac{\sigma^2_{\tilde{X},\Delta t}}{(T/\tau)}$ where $\sigma^2_{\tilde{X},\Delta t} \equiv \langle \tilde{X}^2(\mathbf{w})\rangle_{\substack{\infty\\ \Delta t}} - \langle \tilde{X}(\mathbf{w})\rangle^2_{\substack{\infty\\ \Delta t}}$ is the variance of the operator.[24]

Sampling error is reduced by sampling as many uncorrelated states as possible, and so a timestep Δt comparable to or greater than the correlation time is ideal.

In addition to sampling error, the use of a numerical scheme for time integration introduces systematic error relative to the continuous time equations, which manifests as time discretization error in infinite-time averages:

$$\langle \tilde{X}(\mathbf{w})\rangle_{\substack{\infty\\ \Delta t}} = \langle \tilde{X}(\mathbf{w})\rangle + E^d_{\tilde{X}}(\Delta t). \tag{47}$$

The discretization error $E^d_{\tilde{X}}(\Delta t)$ will depend on the time integration scheme and generally has the form $E^d_{\tilde{X}}(\Delta t) \sim \Delta t^m$, where the exponent m is the "weak" order of accuracy of the stochastic scheme.

Given both these error sources, efficient CL sampling requires using Δt as close to the correlation time as is possible without introducing unacceptably large time discretization error. For some update schemes, timestep size may also be constrained by stability, with $\mathbf{w}(t)$ following a divergent trajectory if an insufficiently small timestep is used. Efficient CL simulation therefore requires algorithms that are both stable and exhibit low discretization error when operating at times comparable to the correlation time.

Initial applications of complex Langevin to polymer field theory used the Euler-Maruyama algorithm, a simple fully explicit scheme of first order weak accuracy that unfortunately is stable only for very small timesteps. Subsequently, Lennon *et al.*[14] showed that stability could be improved by semi-implicit splitting methods. They found that a first-order semi-implicit splitting algorithm ("1S") was stable for very large Δt, but also introduced significant time discretization error for large timesteps. They also tested a second-order semi-implicit splitting algorithm ("2S") and found it offered improved stability compared to EM but not the essentially unlimited stability of 1S; however, 2S offered excellent accuracy up to its stability limit. The EM and 1S schemes are nearly identical in computational cost per timestep, while the 2S scheme is a predictor-corrector approach that is roughly double the cost per timestep of the EM and 1S schemes and requires additional data overhead for calculating single-chain partition functions necessary for the corrector step.

The semi-implicit splitting methods explored by Lennon *et al.* improve stability by treating linear terms in the complex Langevin "force" at an advanced timestep; high-frequency modes of these linear terms are known to have a destabilizing effect that is reduced when treated implicitly in this manner. Exponential differencing algorithms also treat linear terms in an advanced-time manner through incorporation into an integration factor; in the study of ordinary differential equations, these algorithms are known to offer good stability and accuracy properties when applied to stiff equations.[25] In the study of stochastic differential equations, local linearization schemes that incorporate exponential integration factors have also been shown to offer excellent stability for stiff SDEs.[26–28]

We now describe an exponential time differencing scheme of weak first order, which we call ETD1. With the same computational cost per timestep as EM and 1S, the ETD1 scheme offers the appealing stability properties of the 1S algorithm while also offering substantially improved accuracy for large timesteps. Indeed, despite having a lower order of accuracy than the 2S algorithm, in practice the ETD1 algorithm achieves comparable accuracy at large timesteps for the GREM while also offering improved stability.

These schemes all require separate treatment of the linear part of the nonlinear forcing terms in the complex Langevin equations. These linearized terms are diagonal in Fourier rather than in real space, and hence it is most convenient to consider the Fourier-transformed CL equations:

$$\frac{\partial \hat{w}_{\mathbf{k}}}{\partial t} = -\lambda \hat{F}_{\mathbf{k}}(\mathbf{w}(t)) + \hat{\eta}_{\mathbf{k}}(t), \tag{48}$$

where for compactness we have defined $F_{\mathbf{r}}(\mathbf{w}) = \frac{1}{\Delta \tilde{V}} \frac{\partial H(\mathbf{w})}{\partial w_{\mathbf{r}}}$. As the noise $\eta_{\mathbf{r}}$ is a Gaussian random variable, the real and imaginary components of its Fourier transform $\hat{\eta}_{\mathbf{k}} = \hat{\eta}^R_{\mathbf{k}} + i\hat{\eta}^I_{\mathbf{k}}$ are also Gaussian random variables, with zero mean and the moments

$$\left\langle \hat{\eta}^{\alpha}_{\mathbf{k}}(t)\, \hat{\eta}^{\beta}_{\mathbf{k}'}(t')\right\rangle = \lambda\, \tilde{V}\, \delta(t-t') E^{\alpha\beta}_{\mathbf{k},\mathbf{k}'}, \tag{49}$$

where we have defined

$$\begin{aligned} E^{R,R}_{\mathbf{k},\mathbf{k}'} &= \delta_{\mathbf{k},\mathbf{k}'} + \delta_{\mathbf{k},-\mathbf{k}'},\\ E^{I,I}_{\mathbf{k},\mathbf{k}'} &= \delta_{\mathbf{k},\mathbf{k}'} - \delta_{\mathbf{k},-\mathbf{k}'},\\ E^{R,I}_{\mathbf{k},\mathbf{k}'} &= 0. \end{aligned} \tag{50}$$

Note that $\eta_{\mathbf{r}}$ is purely real, and so $\hat{\eta}_{\mathbf{k}}$ are only independent for a half space of $\mathbf{k}$; the number of independent random variables remains unchanged at M.

We define $c_{\mathbf{k}}$ to be the linear Taylor coefficient of $\hat{F}_{\mathbf{k}}$, $c_{\mathbf{k}} \equiv \frac{\partial \hat{F}_{\mathbf{k}}}{\partial \hat{w}_{\mathbf{k}}}|_{\hat{w}_{\mathbf{k}}=0}$, and assume the form c_k, dependent only on the magnitude of the wavevector. This is a consequence of the fact that the linear force kernel is the response function of a chain in zero field, which is rotationally invariant; its Fourier transform is thus dependent only on the magnitude of $\mathbf{k}$. We can then write the ETD1 scheme as

$$\hat{w}^{n+1}_{\mathbf{k}} = \hat{w}^n_{\mathbf{k}} - \frac{1-e^{-\lambda \Delta t\, c_k}}{c_k} \hat{F}_{\mathbf{k}}(\mathbf{w}^n) + \left(\frac{1-e^{-2\lambda \Delta t\, c_k}}{2\lambda \Delta t\, c_k}\right)^{1/2} \hat{R}^n_{\mathbf{k}}, \tag{51}$$

where $\hat{R}^n_{\mathbf{k}} = \hat{R}^{n,R}_{\mathbf{k}} + i\hat{R}^{n,I}_{\mathbf{k}}$ has real and imaginary parts that are Gaussian random variables with moments

$$\left\langle \hat{R}^{n,\alpha}_{\mathbf{k}}\, \hat{R}^{n',\beta}_{\mathbf{k}'}\right\rangle = \lambda \Delta t\, \tilde{V}\, \delta_{n,n'} E^{\alpha\beta}_{\mathbf{k},\mathbf{k}'}. \tag{52}$$

Random variables with these properties can be generated by standard random number generation methods.

For comparison, the semi-implicit 1S algorithm is given by

$$\hat{w}^{n+1}_{\mathbf{k}} = \hat{w}^n_{\mathbf{k}} - \frac{\lambda \Delta t}{1+\lambda \Delta t\, c_k} \hat{F}_{\mathbf{k}}(\mathbf{w}^n) + \frac{1}{1+\lambda \Delta t\, c_k} \hat{R}^n_{\mathbf{k}} \tag{53}$$

and the 2S algorithm is given by

$$\bar{w}_{\mathbf{k}} = \hat{w}^n_{\mathbf{k}} - \lambda\Delta t\, \hat{F}_{\mathbf{k}}(\mathbf{w}^n) + \hat{R}^n_{\mathbf{k}},$$
$$\hat{w}^{n+1}_{\mathbf{k}} = \hat{w}^n_{\mathbf{k}} - \frac{\lambda\Delta t}{1+\frac{\lambda\Delta t\, c_k}{2}} \frac{\hat{F}_{\mathbf{k}}(\bar{\mathbf{w}}) + (1+\lambda\Delta t\, c_k)\hat{F}_{\mathbf{k}}(\mathbf{w}^n)}{2} + \hat{R}^n_{\mathbf{k}}, \tag{54}$$

where in the latter scheme, the same randomly generated values $\hat{R}^n_{\mathbf{k}}$ are used in computing both predictor and corrector steps. As the coefficient λ only acts to rescale the time coordinate, we henceforth fix $\lambda = 1$.

All of these schemes improve stability by treating the linear part of the force, $c_k\, \hat{w}_{\mathbf{k}}$, at an advanced timestep. In the 1S and 2S schemes, this term is directly treated as $c_k\, \hat{w}^{n+1}_{\mathbf{k}}$, whereas in the ETD1 scheme it is incorporated in an integrating factor when integrating the CL equations from time t to $t + \Delta t$. We note that these CL schemes do not require the overall force to be approximately linear in order to recover the exact CL equations in the continuous time limit, but the stability and accuracy of the schemes for finite Δt is expected to improve with the accuracy of the linear approximation.

For the GREM, the forces and linear approximations appearing in these algorithms are

$$\hat{F}_{\mathbf{k}}(\mathbf{w}) = \frac{1}{B}\hat{w}_{\mathbf{k}} + i\,\hat{\Gamma}_{\mathbf{k}}\,\tilde{\rho}_{\mathbf{k}}(\mathbf{w}), \tag{55}$$

$$c_k = \frac{1}{B} + C(1-\delta_{k,0})\,\hat{g}_D(k^2)\,e^{-\alpha^2 k^2}, \tag{56}$$

where $\tilde{\rho}_{\mathbf{k}}(\mathbf{w})$ is the Fourier transform of the density operator defined in Appendix A, and c_k is computed from its weak inhomogeneity approximation. In Sec. IV, we compare the numerical performance of the ETD1 scheme to the 1S and 2S schemes when applied to the GREM.

IV. RESULTS

In Secs. II A and III B, we introduced a regularized field-theoretic model of polymer solutions, and an exponential differencing scheme for complex Langevin field theoretic simulation. In this section, we begin by demonstrating the excellent accuracy and stability properties of the exponential differencing scheme for the GREM. We then use field-theoretic simulations powered by this scheme to investigate the behavior of this model as the lattice spacing is adjusted, and confirm that it has a convergent continuum limit. Further analyzing this lattice discretization data, we demonstrate the superior numerical performance of the ultraviolet-insensitive osmotic pressure operator over its ultraviolet-sensitive counterpart. Finally, we perform an illustrative calculation of osmotic pressure as a function of concentration using field-theoretic simulation of the GREM. These results collectively illustrate the value of the model and algorithm refinements we have presented as a platform for the field-theoretic simulation of polymers.

In Figure 2, we compare the accuracy of the ETD1 algorithm to the 1S and 2S semi-implicit algorithms investigated by Lennon *et al.*[14] The simulations were conducted in

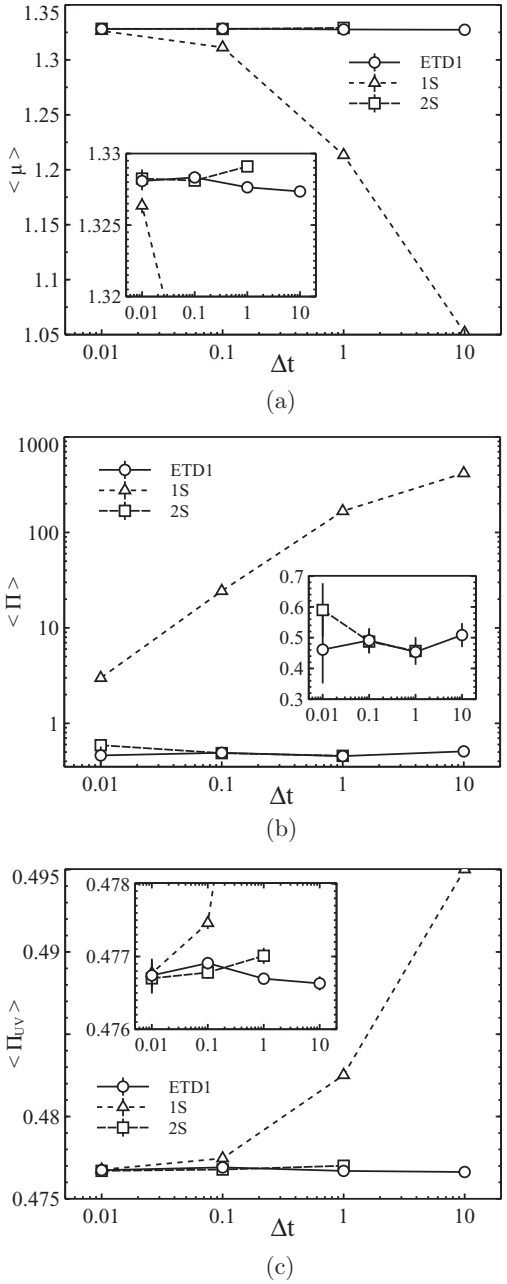

FIG. 2. Comparison of time discretization error in various field theoretic operators calculated via ETD1, 1S and 2S complex Langevin sampling schemes; insets zoom in on identical data. Calculations conducted for $B = C = 1$, $\Delta x = \alpha = 0.1$, $L = 3.2\,R_g$ with contour resolution $\Delta\sigma = 0.01$. Estimated sampling error smaller than symbols or indicated error bars. (a) $\langle\tilde{\mu}\rangle$, (b) $\langle\tilde{\Pi}\rangle$, and (c) $\langle\tilde{\Pi}_{\mathrm{UV}}\rangle$.

three dimensions with $B = C = 1$, $\alpha = 0.1$, and $L = 3.2\,R_g$ with $M = 32^3$ lattice points. Single-chain partition function terms were computed with the fourth-order scheme of Ranjan, Qin, and Morse,[29] briefly outlined in Appendix A, using contour resolution $\Delta\sigma = 0.01$, which was sufficient to reach a continuous contour limit within sampling error. Ensemble averages were calculated for the operators $\tilde{\mu}$, $\tilde{\Pi}$, and $\tilde{\Pi}_{\mathrm{UV}}$, for timesteps $\Delta\tilde{t} = 10, 10^0, 10^{-1}$, and 10^{-2}; the 2S scheme was unstable for $\Delta t = 10$. Correlation times and sampling error for these operators were estimated by blocking,[24] and correlation times were found to range from 0.7 to 1.0 for Δt

$= 10^{-1}$ and 10^{-2}, from 1.2 to 1.7 for $\Delta t = 10^{0}$, and from 10 to 11 for $\Delta t = 10$, indicating an $O(1)$ correlation time in the continuous time equations. After equilibration, the CL equations were integrated for 10^4 timesteps for $\Delta t = 10$ and 1, and for 10^5 timesteps for $\Delta t = 10^{-1}$ and 10^{-2}.

For the $\tilde{\mu}$ and $\tilde{\Pi}_{\mathrm{UV}}$ operators, we see convergence of all algorithms for $\Delta t = 10^{-2}$, indicating that the continuous time limit has been reached. For larger timesteps, we see that the ETD1 and 2S schemes both introduce dramatically less discretization error than the 1S scheme. Indeed, for many applications the latter two schemes may have acceptably low discretization error when sampling at or above the continuous correlation time, thereby permitting highly efficient generation of uncorrelated simulation data.

Although some loss of accuracy for ETD1 and 2S relative to the continuous time limit is apparent for $\Delta t \geq 1$, the 2S algorithm does not appear to give substantially better performance in this regime, and also becomes unstable for sufficiently large timestep, whereas from our testing the ETD1 scheme appears unconditionally stable for this model. Despite being a first-order scheme, the ETD1 scheme thus offers the same practical accuracy benefits as the more costly 2S scheme while also offering improved stability.

Comparing time discretization error in the calculation of $\langle\tilde{\Pi}\rangle$ and $\langle\tilde{\Pi}_{\mathrm{UV}}\rangle$ reveals that elimination of ultraviolet sensitivity also dramatically reduces time discretization error. When using the 1S scheme and the $\tilde{\Pi}$ operator, time discretization error orders of magnitude larger than the continuous-time property of interest are observed, and even for timesteps two orders of magnitude smaller than the continuous correlation time the discretization error is so large as to render the calculation wildly inaccurate. In contrast, the discretization error in the $\tilde{\Pi}_{\mathrm{UV}}$ operator is far smaller, and even for large Δt the 1S scheme provides a correct order-of-magnitude estimate of the osmotic pressure. For the ETD1 and 2S schemes, the large sampling error in calculations using $\tilde{\Pi}$ is far more problematic than the time discretization error.

We now investigate the effects of lattice discretization on the fully fluctuating GREM, as measured by CL simulation. In Figure 3, we plot measured values of $\langle\tilde{\mu}\rangle$, $\langle\tilde{\Pi}\rangle$, and $\langle\tilde{\Pi}_{\mathrm{UV}}\rangle$ for $B = C = 1$, $L = 3.2R_g$ and varying α and lattice resolution Δx. CL simulations were conducted with the ETD1 scheme with $\Delta t = 0.1$, integrating for 5×10^4 timesteps for the $\Delta x = 0.05$ calculations and for 10^5 timesteps for all other calculations.

For $\alpha = 0.1$ and $\alpha = 0.2$, a contour resolution of $\Delta\sigma = 0.1$ was used, while for $\alpha = 0.075$ a contour resolution of $\Delta\sigma = 0.05$ was necessary for convergence to a continuum contour limit (within sampling error). High-resolution complex Langevin simulations of $\alpha = 0$ did not reach the continuum contour limit even for $\Delta\sigma = 1/800$; the exponential smearing function smooths the field input into the single-chain partition function and thus requires lower-accuracy solutions of the modified diffusion equation used to calculate $Q[i\Gamma * w]$.

The CL results for the chemical potential $\langle\tilde{\mu}\rangle$ are within sampling error of the one-loop values presented in Figure 1(a). CL results for the osmotic pressure, as measured by the ultraviolet-insensitive operator $\langle\tilde{\Pi}_{\mathrm{UV}}\rangle$, are lower than the one-loop values, indicating stronger fluctuation corrections to the mean-field value in the fully fluctuating theory. Osmotic pressure values measured by the ultraviolet-sensitive operator $\langle\tilde{\Pi}\rangle$ are in good agreement with the values calculated by $\langle\tilde{\Pi}_{\mathrm{UV}}\rangle$ for large Δx, but exhibit large sampling error that prevents meaningful comparison for small Δx; this is the consequence of ultraviolet sensitivity in the $\tilde{\Pi}$ operator. We see from these results that a lattice resolution of $\Delta x \approx \alpha$ is sufficient to reach the continuum lattice limit in these simulations.

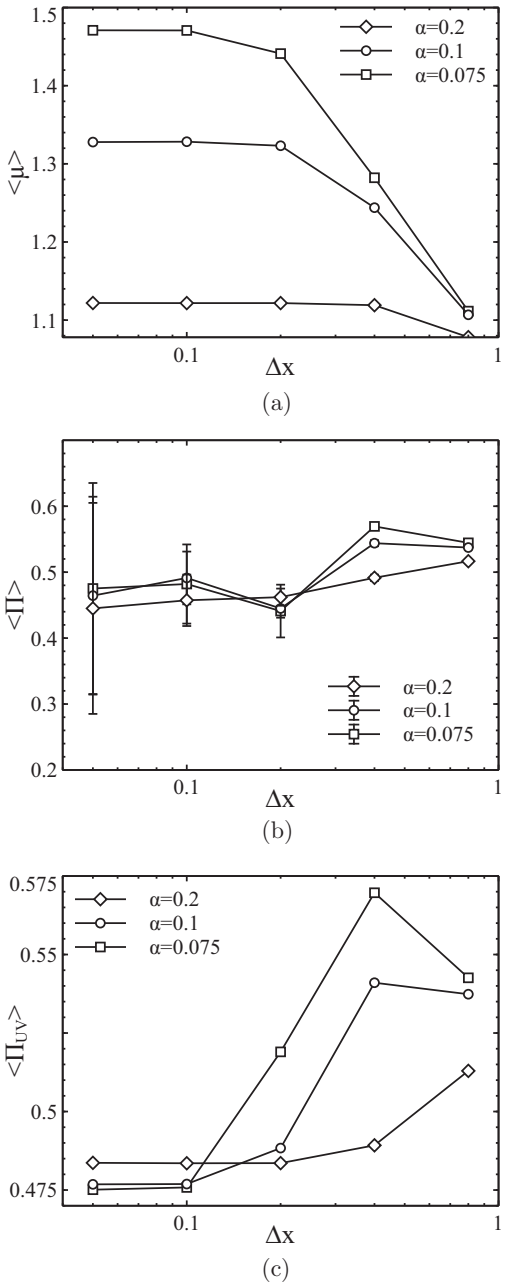

FIG. 3. Lattice discretization effects in chemical potential and osmotic pressure in the GREM as measured by CL simulation, for $B = C = 1$ and $L = 3.2\,R_g$. CL simulations conducted with ETD1 algorithm with timestep $\Delta t = 0.1$, using contour resolution $\Delta\sigma = 0.1$ for $\alpha = 0.2$ and $\alpha = 0.1$, and $\Delta\sigma = 0.05$ for $\alpha = 0.075$. Estimated sampling errors smaller than symbols or indicated error bars. (a) $\langle\tilde{\mu}\rangle$, (b) $\langle\tilde{\Pi}\rangle$, and (c) $\langle\tilde{\Pi}_{\mathrm{UV}}\rangle$.

We now examine the ultraviolet sensitivity properties of the osmotic pressure operators in more detail. As discussed in Sec. III B, the simulation sampling time required to reach

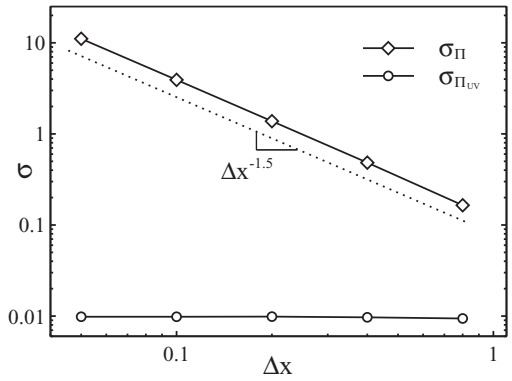

FIG. 4. Comparison of the standard deviations of the standard osmotic pressure operator, $\sigma_{\tilde{\Pi}}$, and the variance of the ultraviolet-sensitivity corrected osmotic pressure operator, $\sigma_{\tilde{\Pi}_{UV}}$, as a function of lattice resolution for $B = C = 1$, $\alpha = 0.1$, and $L = 3.2\,R_g$. $\sigma_{\tilde{\Pi}}$ increases with increasing lattice resolution according to $\sigma_{\tilde{\Pi}} \sim \Delta x^{-1.5}$, thereby introducing additional sampling error. $\sigma_{\tilde{\Pi}_{UV}}$ is independent of lattice resolution.

a desired level of sampling accuracy when calculating an operator average $\langle \tilde{X} \rangle$ is proportional to $\sigma^2_{\tilde{X}} \equiv \langle \tilde{X}^2 \rangle - \langle \tilde{X} \rangle^2$. In Figure 4, we compare measured values of $\sigma_{\tilde{\Pi}}$ and $\sigma_{\tilde{\Pi}_{UV}}$ as a function of lattice resolution for $B = C = 1$, $\alpha = 0.1$, and $L = 3.2\,R_g$, using the same simulation data as presented in the preceding lattice discretization effect analysis.

We find that $\sigma_{\tilde{\Pi}}$ increases strongly with lattice resolution, with the data obeying a power law $\sigma_{\tilde{\Pi}} \sim \Delta x^{-1.5}$. High-resolution simulations would therefore need to increase sampling time by a factor of Δx^{-3} to maintain the same level of accuracy. When combined with the $\Delta x^{-3} \log \Delta x$ increase in computational effort required for calculating field updates for the larger simulation lattice, the total computational effort scales as $O(\Delta x^{-6} \log \Delta x)$! In contrast, $\sigma_{\tilde{\Pi}_{UV}}$ is unaffected by resolution, and furthermore is more than an order of magnitude smaller than $\sigma_{\tilde{\Pi}}$ even for the large lattice resolution of $\Delta x = 0.8$. The elimination of ultraviolet sensitivity thus reduces the computational effort required to accurately calculate the osmotic pressure by many orders of magnitude.

In Figure 5, we demonstrate the use of this improved osmotic pressure operator by calculating the osmotic pressure as

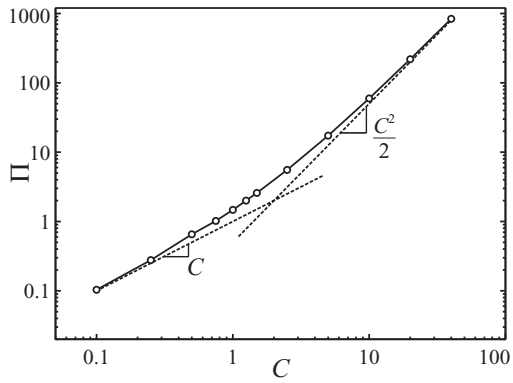

FIG. 5. Osmotic pressure Π vs average polymer concentration C for GREM with $B = 1$, $\Delta x = \alpha = 0.1$, $L = 3.2$. Analytic scalings for the dilute limit, $\Pi \sim C$, and the concentrated limit, $\Pi \sim BC^2/2$, shown for comparison.

a function of concentration C for $a = 0.1$, $L = 3.2\,R_g$, and $\Delta x = 0.1$. All calculations were conducted via ETD1 CL sampling with $\Delta t = 0.1$ and $n = 2 \times 10^4$ timesteps. We observe a transition from the $\Pi \sim C$ scaling of the ideal limit to the $\Pi \sim C^2$ scaling of the concentrated solution limit; interestingly, at this B value we do not observe a large intermediate region with $\Pi \sim C^{9/4}$ semidilute scaling.

V. CONCLUDING REMARKS

In this paper, we have presented a theoretical and numerical framework for the efficient field-theoretic simulations of polymers. In doing so, we have seen that analytic model formulation and numerical performance are tightly linked in field theoretic simulation. By introducing Gaussian interaction potentials that are finite on contact, we obtain ultraviolet-divergence free field theories with well-defined continuum limits in field-theoretic simulation; simulations of these models also require lower contour resolution than the corresponding non-regularized model. The transformation from a given particle-based model to a field theory is non-unique, but we have seen that the choice amongst the infinite spectrum of possible field theories can be consequential for numerical performance: using variable transforms to eliminate ultraviolet sensitivity and to avoid strong amplification of high-frequency modes in CL field update schemes dramatically improves numerical performance. Even with a well-formulated model, the choice of complex Langevin numerical integration scheme has a dramatic impact on performance.

We emphasize that the consequences of such methodological decisions are measured in orders of magnitude of computational expense. For example, compare the calculation of the osmotic pressure of the GREM with $\alpha = \Delta x = 0.1$ and $B = C = 1$ with the $\tilde{\Pi}$ operator and 1S CL sampling against calculation of the same property with the $\tilde{\Pi}_{UV}$ operator and ETD1 CL sampling. As seen in Fig. 2, time discretization errors alone will cause the 1S/$\tilde{\Pi}$ scheme to require timesteps more than two orders of magnitude smaller than the correlation time, while the ETD1 scheme can generate nearly uncorrelated updates with minimal error. Furthermore, the larger variance of the $\tilde{\Pi}$ operator will necessitate four orders of magnitude more uncorrelated data points to obtain the same sampling error as the $\tilde{\Pi}_{UV}$ operator. The inferior method will thus require more than *six orders of magnitude* more compute time - the difference between inexpensive and impossible on typical computational hardware.

The methods described in this paper can be readily used in conjunction with systematic numerical coarse-graining[23] and implemented on graphics processing units.[30,31] We anticipate that such next-generation field theoretic simulation techniques will enable investigation of large, inhomogeneous, fluctuating polymer systems that previously were inaccessible to computational study.

ACKNOWLEDGMENTS

The authors would like to thank Carlos García-Cervera for suggesting the potential utility of exponential differencing algorithms for field theoretic simulations; Robert Riggleman,

Nabil Laachi, Debra Audus, and Kris Delaney for helpful discussion; and Ashley Cooke for contributing to preliminary testing of the ETD1 algorithm. Financial support was provided by NDSEG, NSF GFRP, and NSF DMR CMMT (Grant No. 1160895). We further acknowledge support from the Center for Scientific Computing of the CNSI and MRL: an NSF MRSEC (DMR-1121053), Hewlett-Packard, and NSF CNS-0960316.

APPENDIX A: THE SINGLE-CHAIN PARTITION FUNCTION

The single-chain partition function $Q[W]$ defined in (12) is of central importance in polymer field theory, and calculating it for each field configuration is the most resource-intensive procedure in a field theoretic simulation. An extensive review of the properties of this functional and methods for its calculation is given by Fredrickson;[3] here, we briefly present selected results essential for the above work.

The single-chain partition function is obtained from the chain propagator $q(\mathbf{x}, \sigma; [W])$ according to the relation

$$Q[W] = \frac{1}{\tilde{V}} \int d\mathbf{x}\, q(\mathbf{x}, \sigma = 1; [W]), \tag{A1}$$

where the propagator $q(\mathbf{x}, \sigma; [W])$ is the solution of the modified diffusion equation

$$\frac{\partial}{\partial \sigma} q(\mathbf{x}, \sigma; [W]) = \nabla^2 q(\mathbf{x}, \sigma; [W]) - W(\mathbf{x})\, q(\mathbf{x}, \sigma; [W]) \tag{A2}$$

with initial condition $q(\mathbf{x}, \sigma = 0) = 1$.

When calculating saddle points and field-theoretic forces, the functional derivative $\frac{\delta Q[W]}{\delta W(\mathbf{x})}$ is required; this can be obtained from the chain propagator by

$$\frac{\delta Q[W]}{\delta W(\mathbf{x})} = -\frac{1}{\tilde{V}} \int_0^1 d\sigma\, q(\mathbf{x}, 1-\sigma; [W])\, q(\mathbf{x}, \sigma; [W]). \tag{A3}$$

This functional derivative is also encountered in the calculation of density operators. Following a similar derivation as that provided by Fredrickson for the Edwards model ("Model A")[3], we find that a density operator for the GREM is

$$\tilde{\rho}(\mathbf{x}) = -\frac{n}{Q[i\Gamma * w]} \Gamma * \frac{\delta Q[i\Gamma * w]}{\delta\, i\Gamma * w(\mathbf{x})}. \tag{A4}$$

Although $Q[W]$ cannot be calculated analytically for arbitrary $W(\mathbf{x})$, a variety of approximate techniques are available. The one-loop calculations and semi-implicit linear approximations presented above employ a weak inhomogeneity expansion, which assumes $W(\mathbf{x})$ is only weakly varying from its average value of $\hat{W}_\mathbf{0}/\tilde{V}$ in order to compute the propagator. By expanding in powers of the field, we obtain

$$Q[W] \approx e^{-\hat{W}_\mathbf{0}/\tilde{V}} \left(1 + \frac{1}{2\tilde{V}^2} \sum_{\mathbf{k}\neq\mathbf{0}} \hat{g}_D(k^2)\, \hat{W}_\mathbf{k}\, \hat{W}_{-\mathbf{k}} \right), \tag{A5}$$

$$\mathcal{F}\left[-\frac{1}{Q[W]} \frac{\delta Q[W]}{\delta W(\mathbf{x})} \right]_\mathbf{k} \approx \delta_{\mathbf{k},0} - \frac{1-\delta_{\mathbf{k},0}}{\tilde{V}}\, \hat{g}_D(k^2)\, \hat{W}_\mathbf{k}, \tag{A6}$$

where $\mathcal{F}$ is the Fourier transform operation and $\hat{g}_D(k^2) = \frac{2}{k^4}(e^{-k^2} - 1 + k^2)$ is the Debye function.

In field-theoretic simulations, the chain propagator $q(\mathbf{x}, \sigma; [W])$ is calculated by numerical integration of the modified diffusion equation (A2). This equation can be integrated along the contour variable σ with an efficient pseudo-spectral method based on operator splitting:[32,33]

$$q(\mathbf{x}, \sigma + \Delta\sigma) = e^{-\frac{W(\mathbf{x})}{2}\Delta\sigma} e^{\nabla^2 \Delta\sigma} e^{-\frac{W(\mathbf{x})}{2}\Delta\sigma} q(\mathbf{x}, \sigma) + O(\Delta\sigma^3), \tag{A7}$$

where the $e^{\nabla^2 \Delta\sigma}$ operator is computed by applying a discrete fast Fourier transform (FFT), multiplying each Fourier mode by $e^{-k^2\Delta\sigma}$, and then applying an inverse FFT. This scheme is globally $O(\Delta\sigma^2)$ accurate, and each full propagator calculation has computational cost that scales as $N_\sigma M \log M$, where N_σ is the number of contour steps and M is the number of spatial lattice points.

As was shown by Ranjan, Qin, and Morse,[29] this scheme is particularly well-suited to accuracy improvement by Richardson extrapolation. In this approach, for each timestep $\Delta\sigma$ two propagator updates are computed with the second-order splitting algorithm (A7), one with a single contour step of size $\Delta\sigma$ and the other with two contour steps of size $\Delta\sigma/2$. These two solutions are then summed so as to eliminate the $O(\Delta\sigma^2)$ error:

$$q_R(\mathbf{x}, \sigma + \Delta\sigma) = \frac{4 q_{\Delta\sigma/2}(\mathbf{x}, \sigma + \Delta\sigma) - q_{\Delta\sigma}(\mathbf{x}, \sigma + \Delta\sigma)}{3}. \tag{A8}$$

For a general second-order update scheme, this extrapolation would produce a third-order scheme. However, the second-order splitting update is reversible in σ and hence has vanishing even-order terms in its local Taylor expansion, and therefore has no $O(\Delta\sigma^3)$ global error term. The Ranjan-Qin-Morse scheme is thus globally $O(\Delta\sigma^4)$ accurate, at a computational cost of three times that of a standard second-order splitting update. We use this scheme in all calculations above; detailed performance evaluations in comparison with other pseudospectral schemes have recently been published.[34,35]

To compute $\frac{\delta Q[W]}{\delta W(\mathbf{x})}$, the integral over σ in (A3) is calculated from the numerical $q(\mathbf{x}, n\Delta\sigma; [W])$ by applying Simpson's rule and exploiting the symmetry of the integrand in σ; this integration scheme is $O(\Delta\sigma^4)$ accurate.[36]

APPENDIX B: VOLUME DERIVATIVE OF THE SINGLE-CHAIN PARTITION FUNCTION

The volume derivative $\frac{\partial Q[W]}{\partial \tilde{V}}$ is required for calculation of osmotic pressure operators. This derivative can be calculated by discretization into a Chapman-Kolmogorov equation, differentiation, and a return to the continuum limit;[12] as an alternative, we here present a more elegant Green's function derivation originated by Laachi.[37]

The volume derivative of $Q[W]$ is found by integrating that of the propagator:

$$\frac{\partial Q[W]}{\partial \tilde{V}} = \frac{1}{\tilde{V}} \int d\mathbf{x}\, \frac{\partial q(\mathbf{x}, 1; [W])}{\partial \tilde{V}}. \tag{B1}$$

The propagator is the solution of the modified diffusion equation (A2); from this differential equation we can derive

another differential equation whose solution is the desired propagator volume derivative. To do so, we first rescale the spatial variable in (A2) from $\mathbf{x}$ to $\mathbf{z} = \tilde{V}^{-1/3}\mathbf{x}$:

$$\frac{\partial}{\partial\sigma}q(\tilde{V}^{1/3}\mathbf{z},\sigma;[W]) = \tilde{V}^{-2/3}\nabla_{\mathbf{z}}^2 q(\tilde{V}^{1/3}\mathbf{z},\sigma;[W]) - W(\tilde{V}^{1/3}\mathbf{z})\,q(\tilde{V}^{1/3}\mathbf{z},\sigma;[W]). \tag{B2}$$

We then differentiate both sides of (B2) by $\tilde{V}$ and return to the original $\mathbf{x}$ spatial variable, obtaining

$$\frac{\partial^2 q}{\partial\sigma\,\partial\tilde{V}} = \nabla^2\frac{\partial q}{\partial V} - \frac{2}{3\tilde{V}}\nabla^2 q - W(\mathbf{x})\frac{\partial q}{\partial\tilde{V}} - \frac{\partial W(\mathbf{x})}{\partial\tilde{V}}q. \tag{B3}$$

This expression can be rearranged as a nonhomogeneous partial differential equation in $\frac{\partial q}{\partial\tilde{V}}$

$$\left(\frac{\partial}{\partial\sigma} - \nabla^2 + W(\mathbf{x})\right)\frac{\partial q}{\partial\tilde{V}} = -\frac{2}{3\tilde{V}}\nabla^2 q - \frac{\partial W(\mathbf{x})}{\partial\tilde{V}}q \tag{B4}$$

obeying homogeneous initial condition $\frac{\partial q(\mathbf{x},0)}{\partial\tilde{V}} = 0$.

To solve this nonhomogeneous equation, we use the associated Green's function $g(\mathbf{x},\mathbf{x}',\sigma;[W])$ satisfying

$$\frac{\partial g}{\partial\sigma} + \mathcal{L}_{\mathbf{x}}\,g = 0;\ \ \mathcal{L}_{\mathbf{x}} \equiv -\nabla_{\mathbf{x}}^2 + W(\mathbf{x});\ \ g(\mathbf{x},\mathbf{x}',0) = \delta(\mathbf{x}-\mathbf{x}') \tag{B5}$$

and periodic boundary conditions, which can be formally written as

$$g(\mathbf{x},\mathbf{x}',\sigma;[W]) = e^{-\mathcal{L}_{\mathbf{x}}\sigma}\delta(\mathbf{x}-\mathbf{x}'). \tag{B6}$$

The propagator can be written in terms of this Green's function by

$$q(\mathbf{x},\sigma;[W] = \int d\mathbf{x}'\,g(\mathbf{x},\mathbf{x}',\sigma;[W]) \tag{B7}$$

which satisfies appropriate initial and boundary conditions by construction.

The Green's function can also be used to construct a solution to a nonhomogeneous partial differential equation with forcing function $F(\mathbf{x},\sigma)$:

$$\frac{\partial f(\mathbf{x},\sigma)}{\partial\sigma} + \mathcal{L}\,f(\mathbf{x},\sigma) = F(\mathbf{x},\sigma), \tag{B8}$$

$$e^{-\mathcal{L}_{\mathbf{x}}\sigma}\frac{\partial}{\partial\sigma}(e^{\mathcal{L}_{\mathbf{x}}\sigma}f(\mathbf{x},\sigma)) = \int d\mathbf{x}'\,F(\mathbf{x}',\sigma)\,\delta(\mathbf{x}-\mathbf{x}'), \tag{B9}$$

$$f(\mathbf{x},\sigma) - e^{-\mathcal{L}_{\mathbf{x}}\sigma}f(\mathbf{x},0) = \int_0^\sigma d\sigma'\int d\mathbf{x}'\,F(\mathbf{x}',\sigma')e^{-\mathcal{L}_{\mathbf{x}}(\sigma-\sigma')}\delta(\mathbf{x}-\mathbf{x}'). \tag{B10}$$

Using the homogeneous initial condition $f(\mathbf{x},0) = 0$ and explicitly introducing the Green's function we obtain

$$f(\mathbf{x},\sigma) = \int_0^\sigma d\sigma'\int d\mathbf{x}'\,F(\mathbf{x}',\sigma')\,g(\mathbf{x},\mathbf{x}',\sigma-\sigma'). \tag{B11}$$

Using the symmetry property $g(\mathbf{x},\mathbf{x}',\sigma) = g(\mathbf{x}',\mathbf{x},\sigma)$, valid because our model involves only homopolymer chains, we can express the spatial integral of f in terms of the chain propagator q:

$$\int d\mathbf{x}\,f(\mathbf{x},\sigma) = \int_0^\sigma d\sigma'\int d\mathbf{x}'\,F(\mathbf{x}',\sigma')\int d\mathbf{x}\,g(\mathbf{x}',\mathbf{x},\sigma-\sigma') = \int_0^\sigma d\sigma'\int d\mathbf{x}\,F(\mathbf{x},\sigma')\,q(\mathbf{x},\sigma-\sigma'). \tag{B12}$$

By comparing (B4) with (B8) we immediately obtain

$$\int d\mathbf{x}\,\frac{\partial q(\mathbf{x},\sigma)}{\partial\tilde{V}} = -\int_0^\sigma d\sigma'\int d\mathbf{x}\,q(\mathbf{x},\sigma-\sigma') \times\left(\frac{2}{3\tilde{V}}\nabla^2 + \frac{\partial W(\mathbf{x})}{\partial\tilde{V}}\right)q(\mathbf{x},\sigma') \tag{B13}$$

and thus the desired volume derivative is given by

$$\frac{\partial Q[W]}{\partial\tilde{V}} = -\frac{1}{\tilde{V}}\int d\mathbf{x}\left(\frac{2}{3\tilde{V}}\Phi_\nabla(\mathbf{x};[W]) + \frac{\partial W(\mathbf{x})}{\partial\tilde{V}}\Phi(\mathbf{x};[W])\right), \tag{B14}$$

where we have defined the functions

$$\Phi(\mathbf{x};[W]) \equiv \int_0^1 d\sigma\ q(\mathbf{x},1-\sigma;[W])\,q(\mathbf{x},\sigma;[W]), \tag{B15}$$

$$\Phi_\nabla(\mathbf{x};[W]) \equiv \int_0^1 d\sigma\ q(\mathbf{x},1-\sigma;[W])\,\nabla^2 q(\mathbf{x},\sigma;[W]). \tag{B16}$$

We now consider the forms of $\frac{\partial W(\mathbf{x})}{\partial\tilde{V}}$ encountered in deriving osmotic pressure operators for the GREM. For input field $W(\mathbf{x}) = i\Gamma * w(\mathbf{x})$, the field volume derivative in (B14) is

$$\frac{\partial W(\mathbf{x})}{\partial\tilde{V}} = \frac{\partial}{\partial\tilde{V}}i\int d\mathbf{x}'\,\frac{e^{-\frac{|\mathbf{x}-\mathbf{x}'|^2}{2\alpha^2}}}{(2\pi)^{3/2}\alpha^3}\,w(\mathbf{x}') = \frac{i}{\tilde{V}}\int d\mathbf{x}'\left(1-\frac{|\mathbf{x}-\mathbf{x}'|^2}{3\alpha^2}\right)\frac{e^{-\frac{|\mathbf{x}-\mathbf{x}'|^2}{2\alpha^2}}}{(2\pi)^{3/2}\alpha^3}\,w(\mathbf{x}') \equiv \frac{i}{\tilde{V}}\Gamma_2 * w(\mathbf{x}), \tag{B17}$$

where $\Gamma_2(\mathbf{x}) = (1-\frac{|\mathbf{x}|^2}{3\alpha^2})\Gamma(\mathbf{x})$ is conveniently calculated in Fourier space for convolutions by $\hat{\Gamma}_2(\mathbf{k}) = \alpha^2|\mathbf{k}|^2 e^{-\alpha^2|\mathbf{k}^2|/2}$. For the volume-scaled input field $W_V(\mathbf{x}) = iV^{-1/2}\,\Gamma * \phi(\mathbf{x})$, the additional volume factor alters the expression to

$$\frac{\partial W_V(\mathbf{x})}{\partial\tilde{V}} = \frac{i}{\tilde{V}^{\frac{3}{2}}}\left(\Gamma_2 - \frac{1}{2}\Gamma\right) * \phi(\mathbf{x}). \tag{B18}$$

In numerical computations of the osmotic pressure operator, $\Phi(\mathbf{x};[W])$ is already calculated for use in complex Langevin field updates; $\Phi_\nabla(\mathbf{x};[W])$ is calculated by pseudo-spectral differentiation of the propagator followed by integration by Simpson's rule.

[1] S. Edwards, Proc. Phys. Soc. **85**, 613 (1965).
[2] M. W. Matsen and M. Schick, Phys. Rev. Lett. **72**, 2660 (1994).
[3] G. H. Fredrickson, *The Equilibrium Theory of Inhomogeneous Polymers* (Oxford University Press, New York, 2006).

[4]M. Matsen, in *Soft Matter, Volume 1: Polymer Melts and Mixtures*, edited by G. Gompper and M. Schick (Wiley-VCH, Weinheim, 2006).
[5]G. Parisi, Phys. Lett. B **131**, 393 (1983).
[6]J. R. Klauder, J. Phys. A **16**, L317 (1983).
[7]V. Ganesan and G. Fredrickson, Europhys. Lett. **55**, 814 (2001).
[8]A. Alexander-Katz, A. G. Moreira, and G. H. Fredrickson, J. Chem. Phys. **118**, 9030 (2003).
[9]A. Alexander-Katz, A. G. Moreira, S. W. Sides, and G. H. Fredrickson, J. Chem. Phys. **122**, 014904 (2005).
[10]Y. O. Popov, J. Lee, and G. H. Fredrickson, J. Poly. Sci. B **45**, 3223 (2007).
[11]J. Lee, Y. O. Popov, and G. H. Fredrickson, J. Chem. Phys. **128**, 224908 (2008).
[12]R. A. Riggleman, R. Kumar, and G. H. Fredrickson, J. Chem. Phys. **136**, 024903 (2012).
[13]E. M. Lennon, K. Katsov, and G. H. Fredrickson, Phys. Rev. Lett. **101**, 138302 (2008).
[14]E. M. Lennon, G. O. Mohler, H. D. Ceniceros, C. J. García-Cervera, and G. H. Fredrickson, Multiscale Model. Simul. **6**, 1347 (2008).
[15]S. Edwards, Proc. Phys. Soc. **88**, 265 (1966).
[16]Z.-G. Wang, Phys. Rev. E **81**, 021501 (2010).
[17]R. Wang and Z.-G. Wang, J. Chem. Phys. **135**, 014707 (2011).
[18]N. Goldenfeld, *Lectures on Phase Transitions and the Renormalization Group* (Addison-Wesley, Reading, MA, 1992).
[19]Z.-G. Wang, J. Chem. Phys. **117**, 481 (2002).
[20]P. Grzywacz, J. Qin, and D. C. Morse, Phys. Rev. E **76**, 061802 (2007).
[21]J. Qin and D. C. Morse, J. Chem. Phys. **130**, 224902 (2009).
[22]G. H. Fredrickson, V. Ganesan, and F. Drolet, Macromolecules **35**, 16 (2002).
[23]M. C. Villet and G. H. Fredrickson, J. Chem. Phys. **132**, 034109 (2010).
[24]M. Allen and D. Tildesley, *Computer Simulation of Liquids* (Oxford University Press, New York, 1987).
[25]S. Cox and P. Matthews, J. Comput. Phys. **176**, 430 (2002).
[26]J. Jimenez, I. Shoji, and T. Ozaki, J. Stat. Phys. **94**, 587 (1999).
[27]C. M. Mora, IMA J. Numer. Anal. **25**, 486 (2005).
[28]F. Carbonell, J. Jimenez, and R. Biscay, J. Comput. Appl. Math. **197**, 578 (2006).
[29]A. Ranjan, J. Qin, and D. C. Morse, Macromolecules **40**, 942 (2008).
[30]F. S. Bates, M. A. Hillmyer, T. P. Lodge, C. M. Bates, K. T. Delaney, and G. H. Fredrickson, Science **336**, 434 (2012).
[31]K. T. Delaney and G. H. Fredrickson, Comput. Phys. Commun. **184**, 2102 (2013).
[32]K. Ø. Rasmussen and G. Kalosakas, J. Poly. Sci. B: Poly. Phys. **40**, 1777 (2002).
[33]G. Tzeremes, K. Ø. Rasmussen, T. Lookman, and A. Saxena, Phys. Rev. E **65**, 041806 (2002).
[34]P. Stasiak and M. Matsen, Eur. Phys. J. E **34**, 110 (2011).
[35]D. J. Audus, K. T. Delaney, H. D. Ceniceros, and G. H. Fredrickson, Macromolecules **46**, 8383 (2013).
[36]W. H. Press, S. A. Teukolsky, W. T. Vetterling, and B. P. Flannery, *Numerical Recipes: The Art of Scientific Computing*, 3rd ed. (Cambridge University Press, New York, NY, USA, 2007).
[37]N. Laachi, personal communication (2012).